CELL BIOLOGY

Female reproductive life span is extended by targeted removal of fibrotic collagen from the mouse ovary

Takashi Umehara[1,2], Yasmyn E. Winstanley[1], Eryk Andreas[1], Atsushi Morimoto[1], Elisha J. Williams[1], Kirsten M. Smith[1], John Carroll[3], Mark A. Febbraio[4], Masayuki Shimada[2], Darryl L. Russell[1], Rebecca L. Robker[1,3]*

The female ovary contains a finite number of oocytes, and their release at ovulation becomes sporadic and disordered with aging and with obesity, leading to loss of fertility. Understanding the molecular defects underpinning this pathology is essential as age of childbearing and obesity rates increase globally. We identify that fibrosis within the ovarian stromal compartment is an underlying mechanism responsible for impaired oocyte release, which is initiated by mitochondrial dysfunction leading to diminished bioenergetics, oxidative damage, inflammation, and collagen deposition. Furthermore, antifibrosis drugs (pirfenidone and BGP-15) eliminate fibrotic collagen and restore ovulation in reproductively old and obese mice, in association with dampened M2 macrophage polarization and up-regulated MMP13 protease. This is the first evidence that ovarian fibrosis is reversible and indicates that drugs targeting mitochondrial metabolism may be a viable therapeutic strategy for women with metabolic disorders or advancing age to maintain ovarian function and extend fertility.

INTRODUCTION

Females are endowed with a limited number of oocytes that mature within the ovary and are periodically released at ovulation to enable a potential conception. As women age, they experience declining fertility because of diminished ovarian function; yet, this begins in their 30s (*1*, *2*), well in advance of the exhaustion of oocytes that normally occurs in the late 40s (*2*, *3*). The cellular basis by which the ovary undergoes this early functional decline relative to other organs in the body, and when there are still an estimated 10^3 oocytes available (*3*), is a long-standing biological question, and slowing the loss of ovarian function with aging is one of the biggest challenges in reproductive medicine for which there are no clinically proven therapies. As a new strategy to extend female reproductive potential, we investigated cellular pathologies in the ovary that prevent release of the remaining oocytes and tested therapies to facilitate their growth and ovulation.

Oocytes are held in meiotic arrest in the ovary, within follicles that are surrounded by extracellular matrix and embedded within stromal interstitial tissue. Recently, increased collagen deposition, indicative of tissue fibrosis, has been documented in the ovaries of postmenopausal women (*4*, *5*) and animal models of reproductive aging (*5*–*9*). The cellular events that cause ovarian fibrosis are not well defined, and whether this intriguing change in matrix and tissue architecture actively contributes to fertility loss is not understood. It is possible that accumulated collagen with aging constrains follicle growth and prevents ovulation, effectively causing premature failure by barring the release of mature, fertilization-competent oocytes. Thus, we tested whether it was possible to reverse ovarian fibrosis and thereby improve female fertility.

In many tissues, particularly lung and liver, fibrosis is a recognized cause of organ failure. Characterized by excessive extracellular matrix deposition and expansion of connective tissue, fibrosis develops in response to repeated tissue insult and inflammation, and also physiological tissue damage that occurs with aging and obesity (*10*–*12*). Proinflammatory chemokines recruit immune cells, predominantly M1 macrophages, to the site of damage, where subsequent induction of anti-inflammatory signals triggers their differentiation. These M2 macrophages then stimulate collagen production by adjacent fibroblasts, in a process akin to wound healing and scar formation (*13*). The only approved antifibrosis drugs, pirfenidone and nintedanib, which are used to treat advanced pulmonary disease, inhibit inflammatory signaling and can slow fibrosis progression but are not curative or designed for long-term use (*14*, *15*).

We investigated the origins of ovarian fibrosis onset by measuring cellular stress responses and inflammatory mediators that cause collagen deposition, in the context of reproductive aging where there is a precipitous midlife loss of fertility. Independent of aging, obesity in women, particularly in association with insulin resistance or metabolic syndrome, also leads to anovulation and longer time to pregnancy (*16*, *17*). Thus, we examined whether obesity-induced ovarian dysfunction also involved fibrotic extracellular matrix deposition, and compared the mechanisms involved with those induced by aging. We find that obesity causes ovarian fibrosis similar to that of reproductive aging, and reveal that mitochondrial damage in stromal cells is the key causal factor triggering inflammation and fibrosis-induced ovarian decline. By pharmacologically targeting the distinct mechanisms within the cascade, we demonstrate that ovarian fibrosis is acutely reversible and can be alleviated to promote ovulation of healthy oocytes.

RESULTS

Ovarian fibrosis in reproductively aged mice is reversible to increase ovulation capacity

To determine whether it is possible to reverse ovarian fibrosis, reproductively aged mice were treated with drugs that are used clinically to manage pulmonary fibrosis: pirfenidone, an anti-inflammatory, antioxidant agent thought to counteract fibrosis via suppression of

[1]Robinson Research Institute, School of Biomedicine, The University of Adelaide, Adelaide, SA, Australia. [2]Graduate School of Integrated Sciences for Life, Hiroshima University, Higashi-Hiroshima, Japan. [3]Development and Stem Cells Program and Department of Anatomy and Developmental Biology, Monash Biomedicine Discovery Institute, Monash University, Clayton, VIC, Australia. [4]Monash Institute of Pharmaceutical Sciences, Monash University, Parkville, VIC, Australia.
*Corresponding author. Email: rebecca.robker@adelaide.edu.au

TGFβ1 (transforming growth factor–β1), or nintedanib, a small-molecule inhibitor of tyrosine kinases including VEGFR (vascular endothelial growth factor receptor), FGFR (fibroblast growth factor receptor), and PDGFR (platelet-derived growth factor receptor) (*15*, *18*). Specifically, 15-month-old female mice were administered either pirfenidone (via injection or orally) or nintedanib (via injection) and, following this treatment, were given gonadotropins to synchronously stimulate follicle growth (Fig. 1A and fig. S1A). No oocytes were obtained from the untreated reproductively old females as expected; yet, more than half of those given pirfenidone ovulated (Fig. 1B). Furthermore, the ovulated oocytes were viable and, following in vitro fertilization (IVF), developed normally to the blastocyst stage (fig. S1B). Collagen I/III content in the ovaries, measured by Picrosirius red (PSR) staining, an established indicator of fibrosis (*6*), showed that pirfenidone treatment, but not nintedanib, significantly reduced the amount of fibrillar collagen that had accumulated in the tissue of aged mice (Fig. 1, C and D). These results are the first proof of concept that ovarian fibrosis associated with aging can be reversed to improve ovulation and extend female fertility.

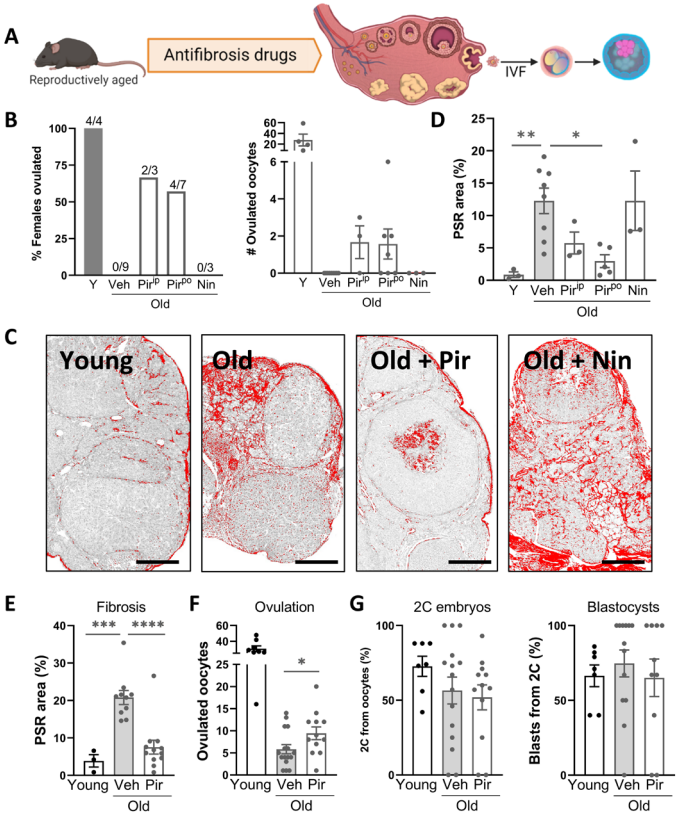

Fig. 1. Pirfenidone reduces ovarian collagen and promotes ovulation in reproductively aged mice. (**A**) Experimental design to test the effects of candidate antifibrosis drugs on ovarian collagen deposition, ovulation, and oocyte developmental competence. (**B** to **D**) Female mice (15 months old) were treated with pirfenidone via injection (250 mg/kg, ip; 4 days) or orally (500 mg/kg, po; 2 weeks) or with nintedinab (50 mg/kg, ip; 4 days) and compared to those treated with vehicle (Veh) and young (Y; 2 months old) controls. Following gonadotropin stimulation, ovaries and oviducts were dissected and ovulation was assessed in each female (B, left) ($n = 3$ to 9 females per group as indicated) and ovulated oocytes were counted (B, right). Ovarian fibrosis was measured by PSR staining of collagen (C and D). Scale bars, 200 μm. (**E** to **G**) Female mice (12 months old) were treated with pirfenidone orally (500 mg/kg; 2 weeks; $n = 12$) or vehicle ($n = 16$) alongside young controls ($n = 8$), and ovarian fibrosis was assessed by PSR strain (E). Ovulated oocytes were counted (F) and subjected to in vitro fertilization, and embryo development was monitored to the two-cell (2C) and blastocyst stage (G). Means ± SEM are shown. $^*P < 0.05$, $^{**}P < 0.01$, $^{***}P < 0.001$, and $^{****}P < 0.0001$ by one-way analysis of variance (ANOVA) (D, E, and G) or two-tailed *t* test (F) compared to vehicle-treated old mice.

We next examined ovaries of mice early in their reproductive aging (at just 12 months old, roughly extrapolating to ~35 years old in women), when fertility decline has commenced (*1*, *2*, *8*) but ovulation failure is not complete. Collagen deposition (more than fivefold above controls) was already apparent in 12-month-old mouse ovaries (Fig. 1E and fig. S2), indicating fibrosis onset at an age that is considerably younger than other previous descriptions that involved mice at 14 to 17 months old (*5*–*7*). Again, pirfenidone treatment (500 mg/kg in drinking water for 2 weeks) reduced ovarian fibrosis (Fig. 1E) and increased the number of oocytes obtained from these reproductively aged females (Fig. 1F). Pirfenidone did not influence ovulation in young mice (fig. S1C), and the ovulated oocytes from young and reproductively aged females, including those treated for 2 weeks with pirfenidone, exhibited normal rates of fertilization and embryo development (Fig. 1G and figs. S1C and S2E). In contrast, a lower dose of pirfenidone or an extended dose of nintedanib was ineffective (fig. S2), as was treatment with olamkicept (sgp130Fc; fig. S3), a fusion protein that targets trans–interleukin-6 (IL-6) signaling to reduce inflammation (*19*, *20*). Thus, although further dose optimization may have yielded effects on fibrosis or ovulation, these two drugs were not pursued further.

Stimulating mitochondrial bioenergetics reverses ovarian fibrosis and functional decline

Altered bioenergetics due to mitochondrial dysfunction is emerging as a key driver of cellular stress and chronic inflammation that can lead to fibrosis (*10*, *21*–*23*). Thus, in parallel to these antifibrosis compounds that target inflammatory pathways, we also tested the efficacy of BGP-15 [(*O*-[3-piperidino-2-hydroxy-1-propyl]-nicotinic amidoxime)] (*24*), a hydroximic acid taken orally in clinical trials (*25*) that has shown efficacy as an insulin sensitizer (*26*) and has been demonstrated to improve mitochondrial function in multiple disease models (*27*–*29*), some of which are accompanied by a reduction in collagen deposition (*28*–*30*). Treatment of 14-month-old female mice with BGP-15 (100 mg/kg) in drinking water for 2 weeks plus injection immediately before ovulation (Fig. 2A and fig. S4) significantly reduced ovarian fibrosis measured by both collagen immunohistochemistry and PSR staining (Fig. 2, B to D). BGP-15 treatment of the reproductively old females also increased the number of oocytes ovulated in response to gonadotropins (Fig. 2E), doubling the average of 2.3 oocytes per female in old mice to 5.5 in those treated with BGP-15. Ovulated oocytes were viable and, following fertilization, developed to the blastocyst stage similar to untreated controls (Fig. 2F). BGP-15 had no effect on ovulation in young mice (fig. S4C). Together, these results demonstrate that ovarian fibrosis is an early event in female reproductive decline and that age-induced ovarian fibrosis is reversible, leading to an improved capacity for ovulation and potential conception.

To understand whether mitochondrial dysfunction is an underlying factor in ovarian fibrosis, we examined ovarian stromal cell bioenergetics and stress responses with aging. Stromal cells were isolated from ovaries (Fig. 3, A and B) and examined for both age- and

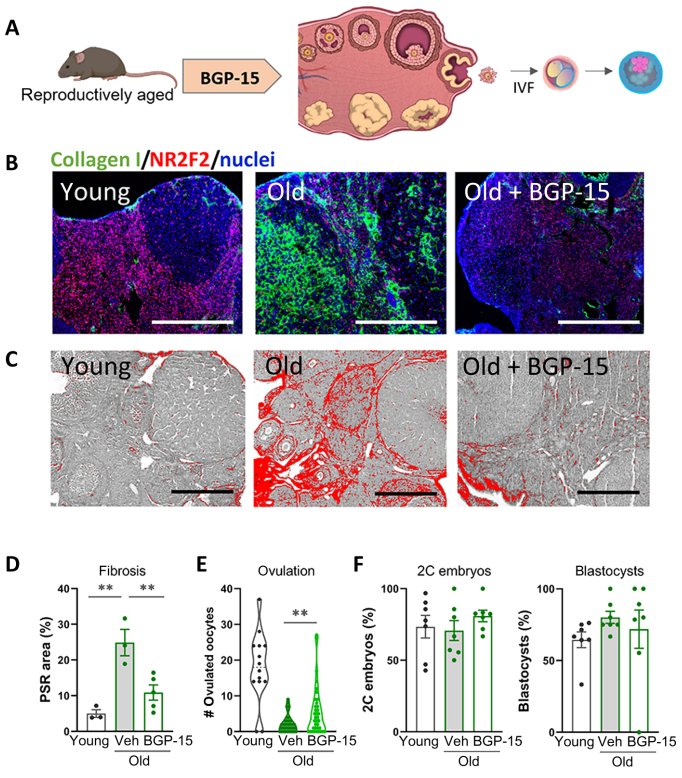

Fig. 2. BGP-15 reduces ovarian collagen and promotes ovulation in reproductively aged mice. (**A**) Experimental design in which female mice were treated with BGP-15 (100 mg/kg; in drinking water for 2 weeks plus intraperitoneal injection for 4 days immediately before ovulation; $n = 36$) or vehicle ($n = 35$) alongside young controls ($n = 14$), followed by assessments of ovarian fibrosis, ovulation, and oocyte developmental competence. At 14 months of age, ovaries were collected following gonadotropin stimulation and fibrosis was measured in sections from $n = 3$ to 5 mice per group by immunohistochemistry for collagen type I (green) and stromal cell marker NR2F2 (red) plus 4′,6-diamidino-2-phenylindole (DAPI) nuclear counterstain (blue) (**B**) and PSR staining (**C** and **D**). Scale bars, 200 μm. Ovulated oocytes were counted in all mice (**E**), pooled into groups of three to six, and subjected to in vitro fertilization and embryo development monitored to the two-cell and blastocyst stage (**F**). Means ± SEM are shown. $^{**}P < 0.01$ by one-way ANOVA (D and F) or two-tailed *t* test (E) compared to vehicle-treated old mice.

BGP-15–induced changes within the ovarian stromal compartment. Metabolic profiling showed that ovarian stromal cells from reproductively old females (14 months) exhibited reduced mitochondrial respiration, glycolysis, and fatty acid oxidation (Fig. 3, C to E). BGP-15 treatment of old mice (100 mg/kg; 2 weeks in drinking water plus injection immediately before ovulation) improved stromal cell maximal respiration and fatty acid oxidation but did not influence glycolysis (Fig. 3, C to E), indicating that BGP-15 stimulates mitochondrial bioenergetics in stromal cells. Analysis of gene expression in stromal cells showed only modest changes in mitochondria biogenesis genes (*Nrf1*, *Pgc1a*, and *Tfam*) and no significant dysregulation in a panel of glycolysis-related genes (fig. S5). Adenosine triphosphate (ATP) assays confirmed that, compared to young mice, mitochondrially produced ATP was reduced in stromal cells from old mice but not in those treated with BGP-15 and that glycolysis-derived ATP was less affected (Fig. 3F). Thus, ovarian stromal cells exhibit compromised mitochondrial bioenergetics with aging, which is responsive to therapeutic manipulation.

Obesity induces ovarian fibrosis that is reversible with BGP-15, metformin, or MitoQ

Obesity is a separate physiological context that leads to impaired ovulation in association with metabolic dysregulation, yet whether ovarian fibrosis could be a contributing factor has not been previously investigated. Notably, within the ovary, obesity and aging each induce similar features of mitochondrial dysfunction, endoplasmic reticulum (ER) stress, oxidative stress, lipotoxicity, and inflammation (*31*–*35*). Thus, using young mice that are obese and hyperinsulinemic due to overeating (*35*), we examined whether ovarian fibrosis occurs with obesity and directly compared to the effects of aging. Mice that were either obese (i.e., >36 g) or reproductively aged (12 months) were generated in parallel from the same colony. Analysis of collagen levels in ovaries collected at the time of ovulation [i.e., 15 hours after human chorionic gonadotropin (hCG)] from the obese and reproductively old mice compared to the matched controls found that, unexpectedly, collagen deposition occurred to a similar extent in both (Fig. 4A). Furthermore, an inverse correlation between collagen-positive stromal area and number of ovulated oocytes (Fig. 4B) suggests a causative negative influence of extracellular matrix deposition on ovulatory function. Histological examination confirmed that ovaries of young lean mice have multiple corpora lutea, while, in contrast, large unruptured follicles were observed in the ovaries of both obese and old females (Fig. 4C) (*7*, *35*), highlighting that follicles containing oocytes are present but unable to complete ovulation.

The ability of BGP-15 to reverse fibrosis biomarkers was investigated by treating obese or old mice with BGP-15 for just a single reproductive cycle (4 days) concurrent with gonadotropin stimulation [as in (*35*) and Fig. 4D]. PSR staining intensity was equally high in ovaries of obese and old mice (Fig. 4E), consistent with collagen immunostaining. Treatment of mice with BGP-15 for 4 days decreased ovarian fibrosis (Fig. 4E) in association with ovulation of an increased number of oocytes (Fig. 4F). Young lean control mice that were treated in parallel with BGP-15 did not have any change in ovulation (fig. S4D), demonstrating that BGP-15 does not nonspecifically increase ovulation in all contexts.

We also determined that accumulating tissue damage due to repeated ovarian cycling contributes to ovarian fibrosis and fertility decline in the context of aging. Ovaries of 12-month-old females that were nulliparous virgins, and thus presumably cycled continuously, showed markedly higher PSR^{+} collagen compared to 12-month-old "retired breeders" that were continuously pregnant and hence experienced markedly fewer cycles (Fig. 4G). Ovulation capacity inversely mirrored the pattern of fibrosis. A greater proportion of the high-parity females were still capable of ovulation [90.48% versus 70.32% in nulliparous; $P = 0.007$, Fisher's exact test (two-sided)], and in these females, the number of oocytes ovulated was higher (Fig. 4H). Thus, continuous cycles of follicular rupture and repair, and not just aging per se, are a major contributor to ovarian fibrosis and anovulation. BGP-15 treatment did not alter the proportion of old females that ovulated, but increased the ovulation rate (i.e., number of oocytes ovulated) in both nulliparous and multiparous mice (Fig. 4H).

A large portion of aged females failed to ovulate any oocytes (20 of 54; 37.0%), in contrast to obese females where the majority (34 of 39; 87.2%) did ovulate. Examination of ovarian sections from the anovulatory aged mice showed that the number of large preovulatory-stage follicles was increased in old females treated with BGP-15 (Fig. 4I). This indicates that, even in reproductively old females

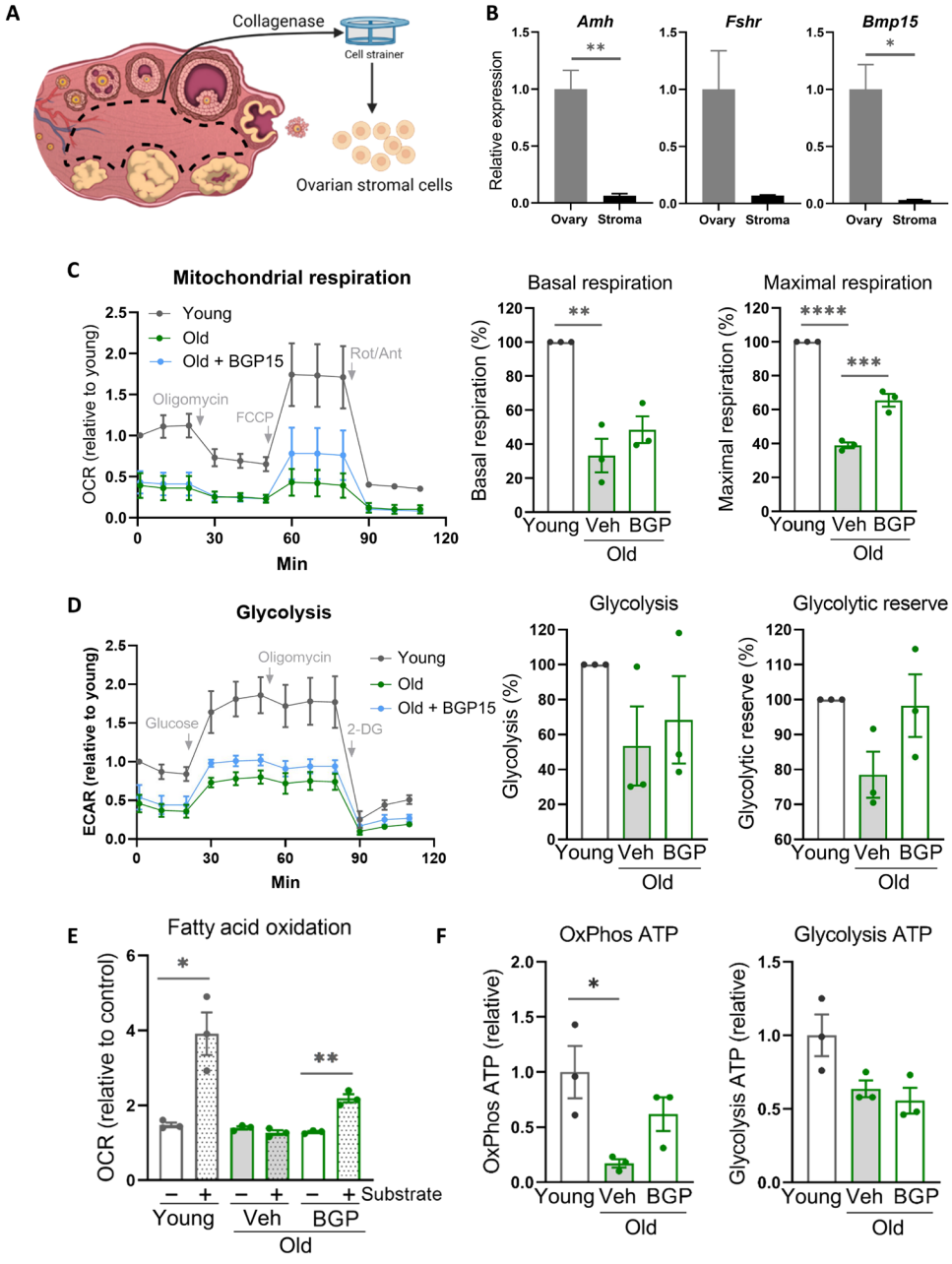

Fig. 3. Ovarian stromal cells of reproductively aged mice exhibit deficient mitochondrial bioenergetics that is improved by BGP-15 treatment. (**A**) Ovarian stromal cells are isolated by microdissection of follicles and corpora lutea from the ovary followed by digestion and filtration. Low expression of granulosa cell (*Amh* and *Fshr*) and oocyte (*Bmp15*) markers is verified (**B**). Ovarian stromal cells were isolated from mice that were young, old (14 months), or old and treated with BGP-15 (100 mg/kg for 2 weeks in drinking water plus intraperitoneal injection for 4 days immediately before ovulation) followed by assessment of mitochondrial respiration (**C**), glycolysis (**D**), fatty acid oxidation (**E**), and ATP levels (**F**). Values represent means ± SEM of $n = 3$ experimental replicates, each using four to six wells containing cells pooled from three to five mice. *$P < 0.05$, **$P < 0.01$, ***$P < 0.001$, and ****$P < 0.0001$ by two-tailed t test (B and E) or one-way ANOVA (C, D, and F) or compared to vehicle-treated old mice.

that failed to ovulate in the current cycle, abundant oocytes were present in the ovaries and capable of growth, in response to BGP-15.

These results demonstrating that ovarian fibrosis and anovulation due to either obesity or aging were reversible with BGP-15 treatment prompted testing of other common mitochondrially targeted therapeutics. Metformin [an activator of AMPK (AMP-activated protein kinase) (*36*)] and MitoQ [a mitochondria-targeted CoQ10 ubiquinone (*37*)] were chosen because of their known therapeutic actions to improve mitochondrial function and their widespread use in humans (*36*, *38*); particularly, metformin is commonly used to treat anovulation associated with insulin resistance.

Mice that were obese or reproductively old were provided with metformin or MitoQ in drinking water for 2 weeks (fig. S6) followed by gonadotropin stimulation and ovulation assessments. Treatment

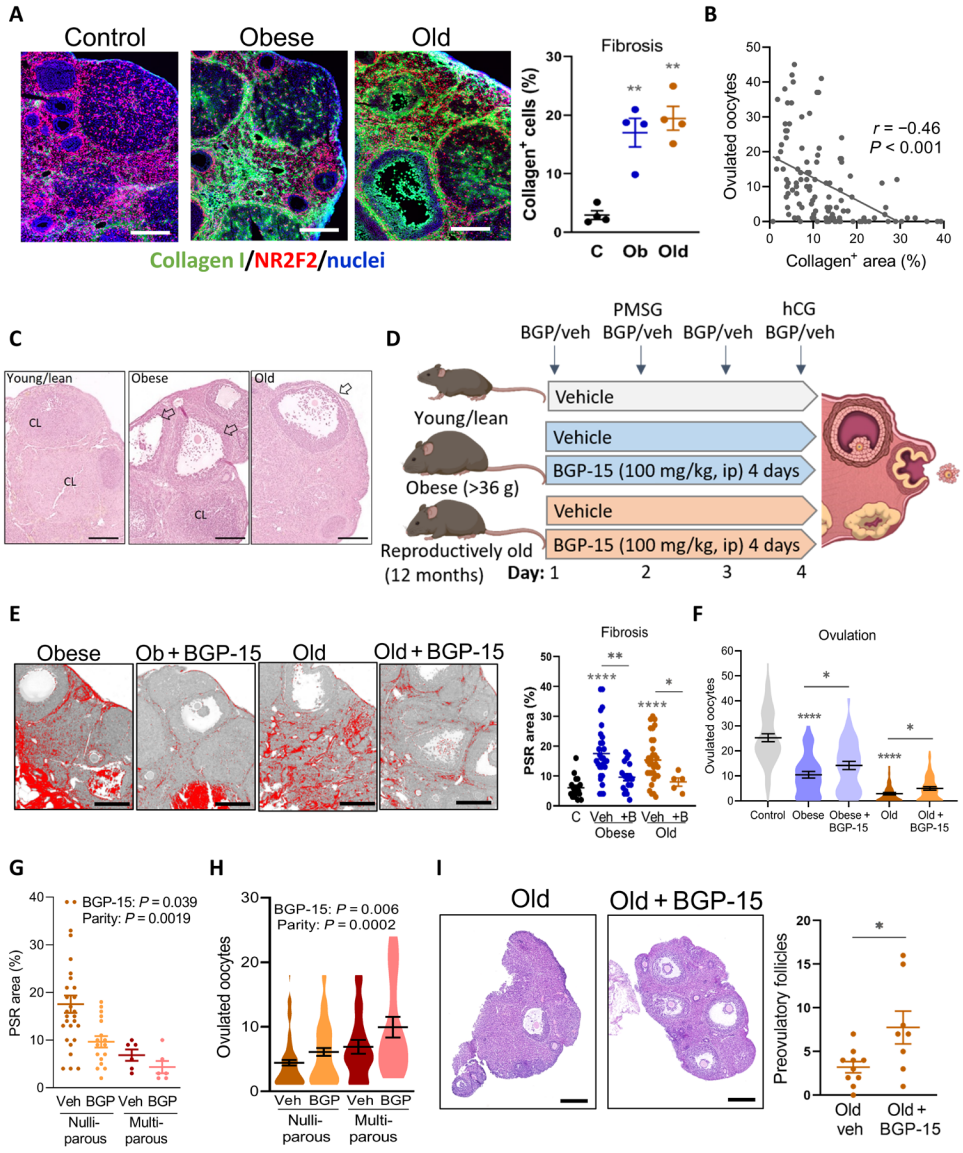

Fig. 4. Obesity and aging cause ovarian fibrosis correlated with ovulation failure, which is mitigated by BGP-15 treatment. (**A**) Left: Collagen localization in ovarian stroma of control (C), obese (Ob), and old mice using anti–collagen type I antibody (green) and anti-NR2F2 antibody (red). Scale bars, 200 μm. Right: Percentage of green (collagen) signal/ovarian stromal area. Means ± SEM of $n = 4$ ovaries (from four mice) per group. (**B**) Correlation (Pearson's test) between fibrosis area and ovulation number in control, obese, and old mice; $n = 111$. (**C**) Representative hematoxylin and eosin histology showing corpora lutea (CL) and ovulatory yet unruptured follicles (arrows). Scale bars, 200 μm. (**D**) Experimental groups and treatments. (**E**) Representative PSR-stained ovarian sections. Scale bars, 200 μm. Fibrosis area quantified (right). Means ± SEM of ovaries from $n = 5$ to 32 mice per group. (**F**) Ovulation in young lean controls ($n = 53$), obese mice treated with saline vehicle ($n = 39$) or BGP-15 ($n = 38$), and old mice treated with vehicle ($n = 54$) or BGP-15 ($n = 57$). Means ± SEM shown within violin plot. (**G**) Collagen content (PSR stain) in ovaries from old mice that were nulliparous ($n = 17$ or 21) or multiparous ($n = 6$ each vehicle-treated and BGP-15–treated mice) and (**H**) ovulation in the same types of mice ($n = 20$ to 79 per group). Effects of parity and BGP-15 identified by two-way ANOVA. (**I**) Representative ovarian sections of old mice that did not ovulate and number of large preovulatory follicles (right). $^*P < 0.05$, $^{**}P < 0.01$, and $^{****}P < 0.0001$ by one-way ANOVA compared to controls or by two-tailed t test compared to vehicle-treated mice, as indicated. Scale bars, 200 μm.

of obese mice with either metformin or MitoQ reversed ovarian fibrosis and normalized the number of oocytes ovulated (Fig. 5, A to C). MitoQ consumption also increased ovarian stromal cell mitochondrial respiration in obese mice (fig. S6). In reproductively aged mice, consumption of metformin or MitoQ also effectively reduced ovarian fibrosis (Fig. 5, D and E). In contrast to the effects in obese mice, these same doses of metformin and MitoQ did not influence ovulation in old females (Fig. 5F); however, it is possible that, with the limited ovarian reserve of these mice and the relatively long treatment time (2 weeks), any transient increase would not have been detected. Similar to BGP-15, MitoQ treatment increased the number of large preovulatory follicles in the ovaries of old mice that failed to ovulate (Fig. 5, G and H), confirming an association between reduced fibrosis and improved development of remaining follicles. These experiments, using well-characterized compounds, further substantiate that targeting cellular bioenergetics reverses ovarian fibrosis.

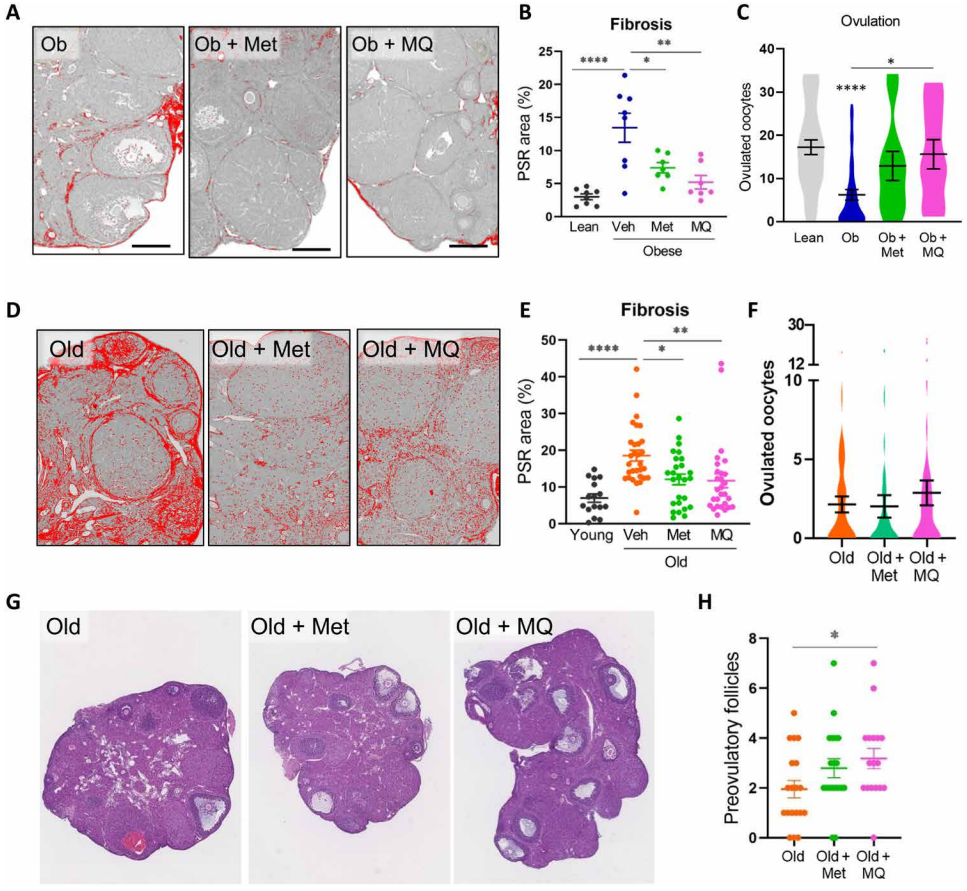

Fig. 5. Metformin and MitoQ reverse ovarian fibrosis in obese and reproductively old mice. Obese (Ob) or reproductively old mice (12 months) were treated with metformin (Met) or MitoQ (MQ) via drinking water or untreated (Veh) and compared to lean/young (4 to 5 months old) controls. (**A**) Representative PSR-stained ovarian sections from obese mice and quantification of fibrosis area in the stroma (**B**). (**C**) Number of oocytes ovulated following gonadotropin stimulation of obese mice and controls. $n = 35$ (Lean), $n = 42$ (Obese), and $n = 11$ (Ob + Met and Ob + MQ). (**D**) Representative PSR-stained ovarian sections from old mice and quantification of stromal fibrosis area (**E**). (**F**) Number of oocytes ovulated in each group of reproductively old females. $n = 44$ (Old), $n = 38$ (Old + Met), and $n = 44$ (Old + MQ). Young females ovulated 21.0 ± 2.8 oocytes. (**G**) Preovulatory follicles were counted in ovarian sections of old females that failed to ovulate. (**H**) $n = 19$ (Old and Old + Met) and $n = 17$ (Old + MQ). Means ± SEM are shown. $^*P < 0.05$, $^{**}P < 0.01$, and $^{****}P < 0.0001$ by one-way ANOVA compared to lean/young controls or compared to untreated (Veh) mice as indicated (B, C, and E to G).

BGP-15 reverses mitochondrial dysfunction, oxidative damage, and ER stress

The causative cellular mechanisms leading to ovarian fibrosis and its association with anovulation were sought through comprehensive analysis of biomarkers of the fibrosis cascade. Specifically, mitochondrial dysfunction and intracellular stress pathways that induce inflammation [oxidative stress, ER stress, and lipotoxicity (*11*, *12*, *39*, *40*)] were examined within the ovarian stroma of obese and reproductively old mice and those treated with BGP-15 for 4 days before ovulation. Mitochondrial metabolic dysfunction in stromal cells of both obese mice and 12-month-old mice was improved by BGP-15 treatment for 4 days (Fig. 6A). In particular, maximal respiration and spare capacity were decreased in stromal cells from obese or old ovaries compared with controls and recovered by BGP-15 treatment (Fig. 6B). Consistent with these findings, mitochondrial membrane potential in ovarian stromal cells, measured by JC-1 potentiometric dye and flow cytometry (fig. S7), was lower in cells from both obese and old females compared with controls (Fig. 6C), indicative of altered electron transport chain function and reduced respiratory capacity. In contrast, mitochondrial oxidative stress and reactive oxygen species (ROS) production detected by MitoSOX Red staining was higher in stromal cells of obese or old females (Fig. 6D). Both mitochondrial defects were recovered by in vivo BGP-15 treatment (Fig. 6, C and D). These identical effects of obesity and age on mitochondrial activities and consistent normalization by BGP-15 were not associated with similarly distinct patterns in expression of mitochondria biogenesis and glycolysis regulatory genes (fig. S8), suggestive of direct actions on mitochondrial function rather than transcriptional responses.

Oxidative damage in ovarian tissue, measured by detection of 4-HNE, a marker of lipid peroxidation, showed increased prevalence and colocalized with stromal marker NR2F2 in ovaries of both obese and aged mice (Fig. 6E). BGP-15 treatment markedly decreased 4-HNE staining (Fig. 6E). Oxidative DNA damage was also more frequent in ovarian stroma of obese or old mice and decreased by BGP-15 treatment, as determined by immunofluorescence for 8-OHdG (8-hydroxy-2′-deoxyguanosine), a marker of oxidized guanidine (Fig. 6F). Increased damage in stromal cells was also indicated by activation of the DNA damage repair factor PARP1 [poly(adenosine diphosphate–ribose)

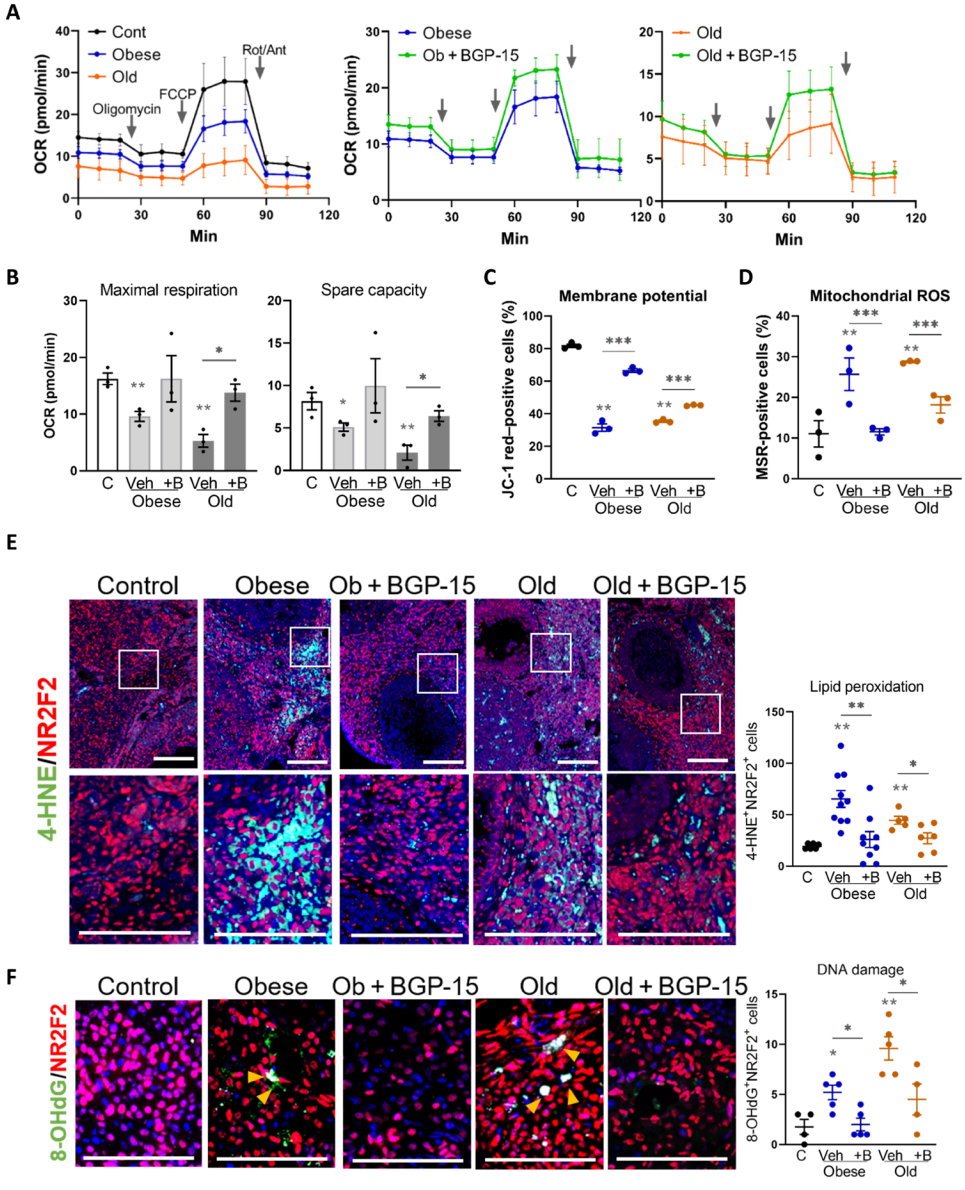

Fig. 6. Mitochondrial dysfunction and oxidative stress in ovarian stroma with obesity or aging are recovered by BGP-15. (**A**) Kinetics of oxygen consumption rate (OCR) in ovarian stromal cells from control mice or those that are obese or old and compared to those from mice treated with BGP-15 using the Seahorse XF Analyzer. Values represent means ± SEM of $n = 3$ experimental replicates, each using four to six wells containing cells pooled from three to five mice. (**B**) Maximal respiration and spare capacity calculated from OCR of ovarian stromal cells from control (C), obese, and old mice with/without BGP-15 (+B) treatment. (**C**) Percent of JC-1 red–positive (high mitochondrial membrane potential) ovarian stroma cells from control, obese, and old mice with/without BGP-15 treatment. (**D**) Percent of MitoSOX Red–positive ovarian stroma cells from control, obese, and old mice with/without BGP-15 treatment. (C and D) $n = 3$ replicates of cells pooled from four to six animals each and analyzed by flow cytometry. (**E**) Localization of oxidized lipid marker 4-HNE (green) in the ovarian stroma of obese and old mice treated with BGP-15 (or vehicle), colocalized with anti-NR2F2 stromal cell marker (red). The boxed area is shown in the bottom panel. Scale bars, 100 μm. Number of 4-HNE and NR2F2 double-positive cells in the ovarian stromal area (right). $n = 5$ to 10 mice per group. (**F**) Localization of oxidized DNA marker 8-OHdG (green) in the ovarian stroma of obese and old mice treated with BGP-15 (or vehicle), colocalized with anti-NR2F2 stromal cell marker (red). 8-OHdG and NR2F2 double-positive cells in the ovarian stromal area (right). $n = 4$ to 5 mice per group. (B to F) $^{*}P < 0.05$, $^{**}P < 0.01$, and $^{***}P < 0.001$ by one-way ANOVA compared to controls or by two-tailed t test between BGP-15–treated and vehicle-treated mice as indicated.

polymerase 1] in a similar pattern to the 8-OHdG–positive cells (fig. S9A). ER stress, defined by changes in marker gene expression (*Atf4*, *Hspa1a*, and *Xbp1s*), was increased in ovarian stromal cells by both obesity and aging and reduced by treatment with BGP-15 (fig. S9B). Thus, obesity and aging both result in a consistent array of cellular stress responses within ovarian stromal cells, namely, impaired mitochondrial respiration, oxidative damage to lipid and DNA, and induction of ER stress. That each of these responses was mitigated by in vivo treatment with BGP-15 suggests that they are downstream of an initiating change in mitochondrial bioenergetics. In contrast, lipid accumulation and multiple lipogenesis marker genes were markedly increased in the ovarian stroma by both obesity and aging but, unlike

the other cellular damage responses, were not affected by BGP-15 treatment (fig. S9, C to E), indicating that these phenotypes are not linked to stromal cell mitochondrial dysfunction and oxidative stress.

Inflammatory phenotypes induced by both obesity and aging are reversed by BGP-15

Typical fibrosis onset in response to chronic cellular stress and/or tissue damage involves induction of chemokine expression and recruitment of proinflammatory (M1) macrophages, followed by production of anti-inflammatory cytokines that shifts macrophage polarization to an alternatively activated (M2) phenotype that characteristically promotes collagen secretion during wound healing (*13*). Expression of inflammatory chemokines—*Ccl2*, *Ccl3*, and *Cxcl2*—was increased in ovarian stroma by obesity and aging, and not diminished by BGP-15 (fig. S10). Proinflammatory cytokines *Tnfa* and *Il6* were highly induced, both mRNA and protein, in the ovarian stroma with obesity and aging, and *Il6* was reduced by BGP-15 treatment in both contexts (Fig. 7, A and B). Inflammatory cytokine *Infg* was also increased with both obesity and aging, particularly elevated in ovarian stroma of old mice, and reduced by BGP-15 treatment (Fig. 7C). *Tgfb1*, an anti-inflammatory cytokine known to promote tissue fibrosis, was increased to a similar degree by both obesity and aging, and reduced by BGP-15 in both contexts (Fig. 7C). *Il4* and *Il13*, cytokines that influence immune cell polarization by inducing macrophage differentiation to M2 (*41*), were also increased in ovarian stroma with obesity and aging (Fig. 7C).

Macrophage numbers ($F4/80^+$) within the ovarian stroma were increased with obesity and aging (Fig. 7, D and E) and, in both contexts, exhibited accumulated lipid (fig. S10C). Macrophages positive for inducible nitric oxide synthase (iNOS), an M1 macrophage marker, were common in stroma of obese and old mice and also in ovaries of mice that were treated with BGP-15 (Fig. 7, F and G). In contrast, cells expressing CD163, an M2 macrophage marker, were prevalent in ovaries of obese and old mice, yet the number of $CD163^+$ was markedly lowered by BGP-15 (Fig. 7, F and G). Stromal cell expression of *iNos* and *Cd163* mRNA showed an identical pattern (fig. S10D), confirming that BGP-15 specifically dampens the M2 macrophage phenotype. These data demonstrate that inflammatory and anti-inflammatory signals that recruit immune cells, as well as cytokines that regulate macrophage polarization, are up-regulated in the ovarian stroma in response to obesity and aging, and are modifiable with BGP-15 treatment. Obesity and aging similarly increase macrophage number and alter phenotype ($iNOS^+$, Nile Red^+, and $CD163^+$), with BGP-15 selectively down-regulating the M2 phenotype marker ($CD163^+$) only. Thus, across the comprehensive analyses comparing the effects of obesity and aging on the ovarian stroma, there were only modest differences in gene expression between the two physiological contexts, while other functional readouts such as collagen staining, metabolism, and inflammation biomarkers were identical.

BGP-15 induces matrix metalloproteinase 13 expression

Expression of collagens and relevant proteases was measured to understand the mechanisms of fibrosis resolution in response to BGP-15. Collagen coding genes *Col1a1*, *Col1a2*, and *Col3a1* were expressed at higher levels in stromal cells of obese and old mice (Fig. 8A), consistent with immunohistochemistry (Fig. 4A) and identifying a transcriptional mechanism of collagen accumulation. Unexpectedly, BGP-15 treatment did not alter gene expression (Fig. 8A), indicating that another mechanism is responsible for collagen removal. Examination of extracellular matrix remodeling enzymes showed that BGP-15 markedly increased the expression of matrix metalloproteinase *Mmp13* (Fig. 8B) but not *Mmp2* or *Mmp9* (fig. S11). Matrix metalloproteinase 13 (MMP13) protein levels were also increased by BGP-15 (Fig. 8C). Localization by immunostaining showed MMP13-expressing cells only sporadically around the ovarian follicles in obese and old mice. In ovaries of mice treated with BGP-15, there was increased signal intensity, and the MMP13-expressing cells were prevalent around the follicles, in the stroma, and near the surface epithelium (Fig. 8D and fig. S11). Colocalization with cell-specific markers showed that MMP13 is expressed by cells that are positive for stromal cell marker NR2F2, but also other NR2F2-negative cell types (Fig. 8E). In some instances, MMP13 colocalized with macrophage marker F4/80 (Fig. 8F). Thus, MMP13 mRNA and protein are induced by BGP-15 and expressed in both stromal cells and macrophages, indicating a potential mechanism for collagen removal and improved ovulation in these mice.

Rotenone diet induces ovarian fibrosis phenotypes similar to obesity and aging

The ovarian stroma of obese and reproductively old females exhibits altered metabolism, oxidative stress, heightened inflammation, and collagen deposition. That each of these cellular pathologies is normalized by BGP-15 suggests that they are linked to underlying defects in mitochondrial bioenergetics. To directly examine the initiating role of mitochondrial dysfunction in the onset of ovarian fibrosis and whether altered bioenergetics alone could be a causative factor, mice were administered a well-defined inhibitor of the mitochondrial respiratory chain and fibrosis phenotypes were examined. Specifically, young lean female mice were fed a diet containing a low dose [150 parts per million (ppm)] of rotenone, an inhibitor of complex I, for 3 weeks followed by standard gonadotropin stimulation (Fig. 9A). This dose is demonstrated to decrease complex I– and complex II–driven respiration without altering oxidative phosphorylation subunit abundance or causing overt physiological effects (*42*).

Young female mice fed the rotenone diet exhibited similar phenotypic changes in the ovarian stroma as were observed in the obese mice and old mice, yet with informative differences. Dampened mitochondrial function was observed, as anticipated, in purified ovarian stromal cells of rotenone-treated mice (Fig. 9B). Furthermore, oxidative damage (4-HNE^+ cells) was visibly increased throughout the stromal region, colocalized with $NR2F2^+$ stromal marker (Fig. 9C), substantiating that oxidative stress is a response to disrupted mitochondrial bioenergetics. In contrast, other stress responses, namely, ER stress markers and lipid accumulation that were present in ovaries of obese and old mice, were not present in ovaries of mice fed rotenone (fig. S12). Similarly, inflammatory cytokines were either not detectable (*Tnfa*, *Il4*, *Il13*, and *Infg*) or not induced above control levels (*Il6* and *Tgfb1*; fig. S12). Consistent with this, $F4/80^+$ macrophages were not increased in the ovarian stroma with rotenone (Fig. 9D and fig. S12), in contrast to the increased numbers observed in response to obesity and aging. However, there were increased numbers of both $iNOS^+$ and $CD163^+$ cells (Fig. 9E). This indicates that an oxidative stress–induced shift in macrophage phenotype is an early event occurring before induction of other inflammatory responses and that macrophage polarization rather than recruitment is affected by the rotenone-induced oxidative damage.

Expression of *Col3a1* (but not *Col1a1* or *Col1a2*) in stromal cells was increased by the rotenone diet (Fig. 9F and fig. S12). Moreover, at the extracellular matrix level, PSR staining of sections revealed a

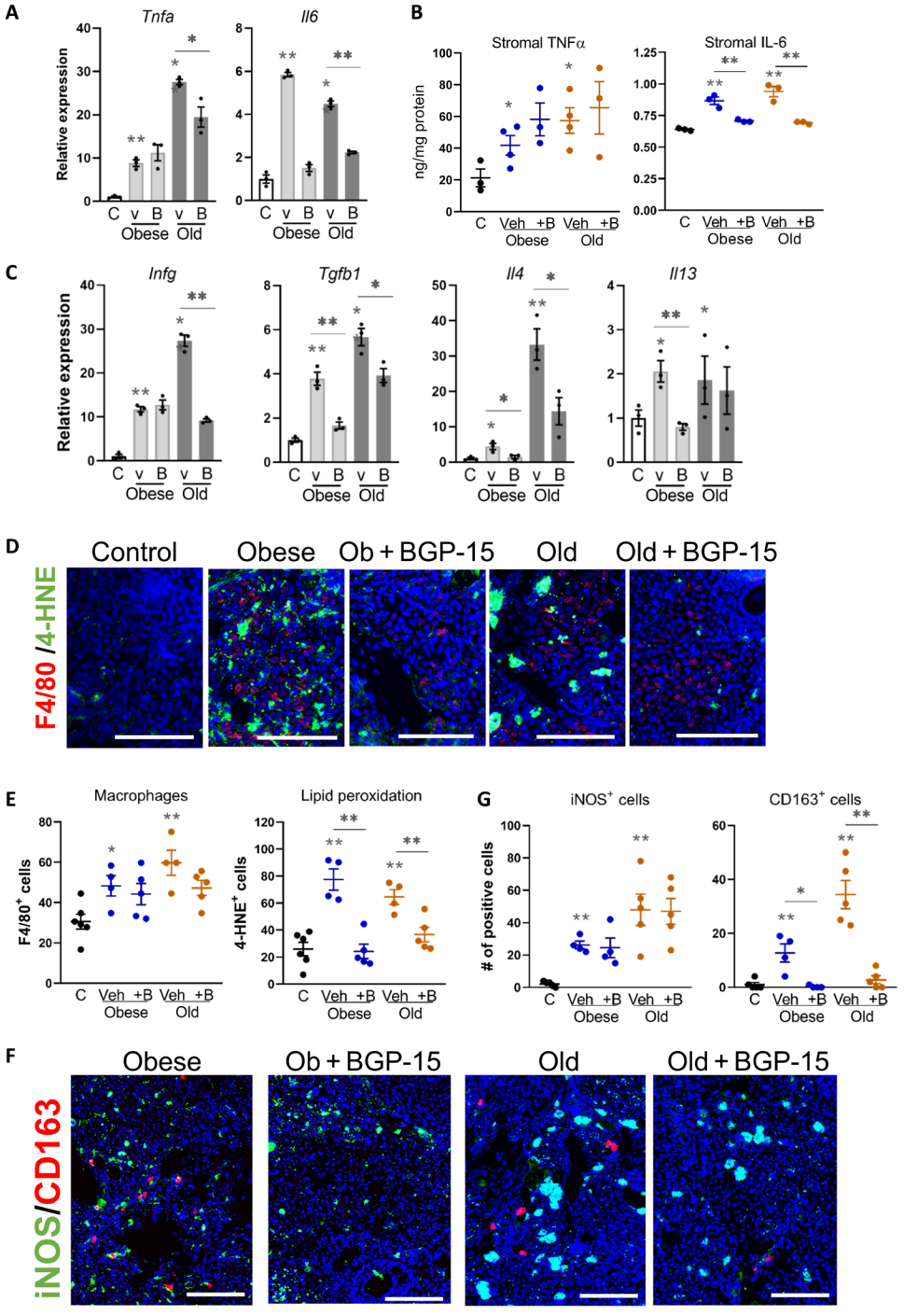

Fig. 7. M1 and M2 inflammation are evident in ovarian stroma with obesity and aging, with M2 macrophage phenotype reduced in BGP-15–treated mice. (**A**) Gene expression of inflammatory cytokines (*Tnfa* and *Il6*) in ovarian stromal cells of control (C), obese, and old mice treated with BGP-15 (B) or vehicle (v). Expression was normalized to *L19* and was presented relative to controls. Values represent means ± SEM of $n = 3$ replicate pools of stromal cells from multiple mice. (**B**) TNFα and IL-6 (normalized to total protein) in ovarian stromal cells. Values represent means ± SEM of $n = 3$ to 4 replicate samples of material pooled from multiple mice. (**C**) Gene expression of *Ifng* and anti-inflammatory cytokines (*Tgfb1*, *Il4*, and *Il13*) in ovarian stromal cells from (A). (**D**) Localization of macrophages in the ovarian stroma using anti-F4/80 antibody (red; macrophages) and anti–4-HNE antibody (green; lipid peroxidation). Scale bars, 100 μm. (**E**) Numbers of F4/80$^+$ (left) or 4-HNE$^+$ (right) cells in the ovarian stroma. (**F**) Localization of iNOS (marker of M1 macrophage; green) and CD163 (marker of M2 macrophage; red) in ovarian stroma by immunohistochemistry. Scale bars, 100 μm. (**G**) Number of iNOS$^+$ or CD163$^+$ cells within the area of ovarian stroma. *$P < 0.05$ and **$P < 0.01$ by one-way ANOVA compared with controls or by two-tailed *t* test compared to vehicle-treated mice as indicated.

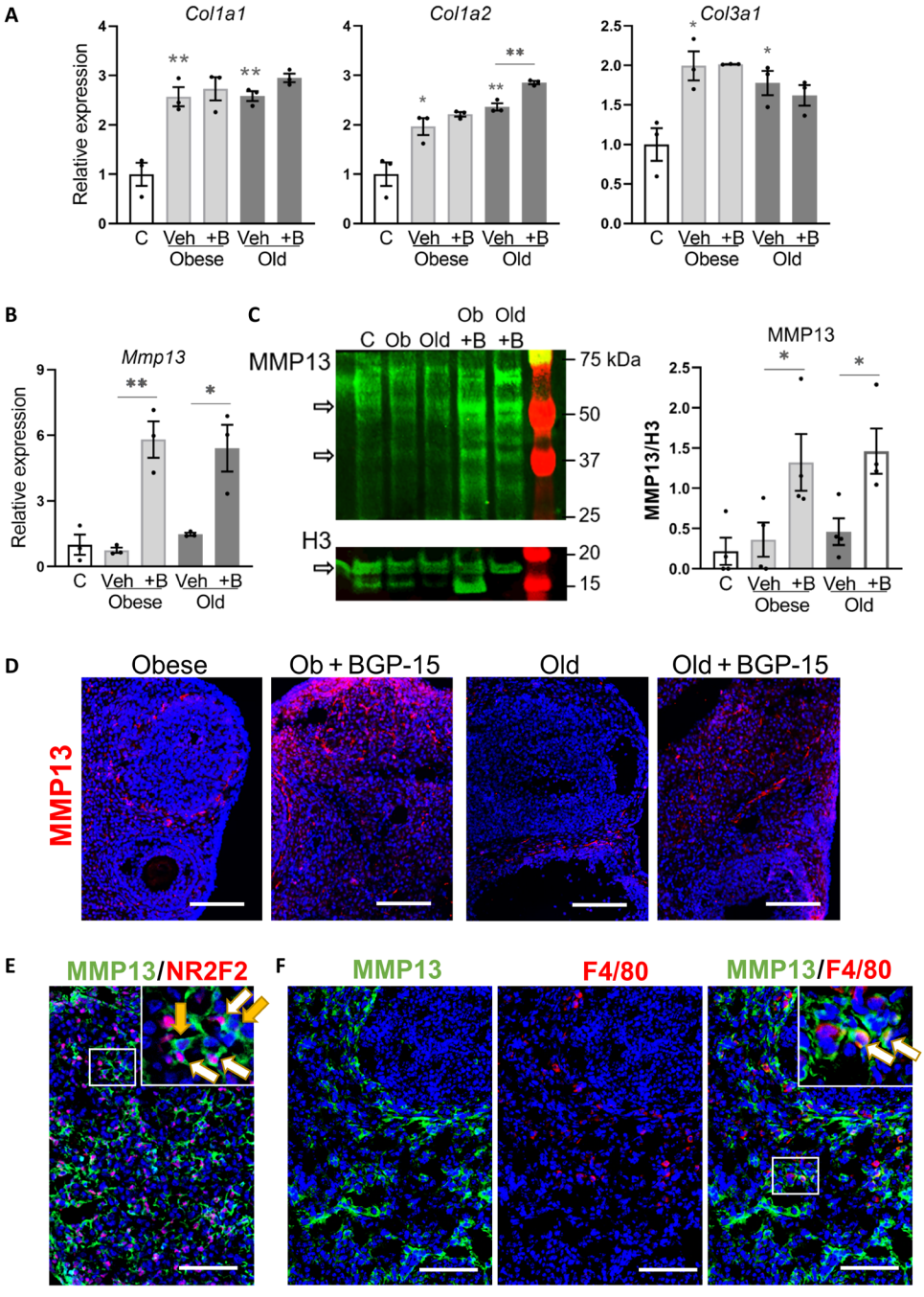

Fig. 8. Increased MMP13 metalloprotease expression in ovarian stroma following BGP-15 treatment. (**A**) Gene expression of collagen-encoding genes (*Col1a1*, *Col1a2*, and *Col3a1*) in ovarian stromal cells of control (C), obese, and old mice treated with BGP-15 (+B) or vehicle (veh). Expression was normalized to *L19* and presented relative to controls. (**B**) Expression of MMP *Mmp13* in the same samples. Values represent means ± SEM of $n = 3$ replicate pools of stromal cells from multiple mice. (**C**) Western blot of MMP13 in ovarian stromal cells of mice as above. Histone H3 is used as a loading control. Active MMP13-positive bands were 48 and 60 kDa. Histone H3–positive band was 17 kDa. Quantification of MMP13 Western blots (right) by measuring the intensity of MMP-13–specific bands normalized to H3. Values are means ± SEM of $n = 4$ replicate Western blots using different pools of stromal cells each collected from multiple mice. $^*P < 0.05$ and $^{**}P < 0.01$ by one-way ANOVA compared with controls or by two-tailed *t* test compared with vehicle-treated mice as indicated. (**D**) Representative sections showing localization of MMP13 in ovaries by immunohistochemistry using anti-MMP13 antibody (red) and DAPI (blue) nuclear counterstain. Scale bars, 100 μm. (**E**) Immunohistochemical colocalization of MMP13 (green) with stromal cell marker NR2F2 (red) in ovarian sections, with white arrows indicating MMP13 expression in $NR2F2^+$ cells and yellow arrows indicating MMP13 expression in $NR2F2^-$ cells. (**F**) Immunohistochemical colocalization of MMP13 (green) with macrophage marker F4/80 (red) in ovarian sections, with white arrows indicating $F4/80^+$ cells expressing MMP13. Inset images (E and F) are magnification of white boxed area Scale bars, 100 μm.

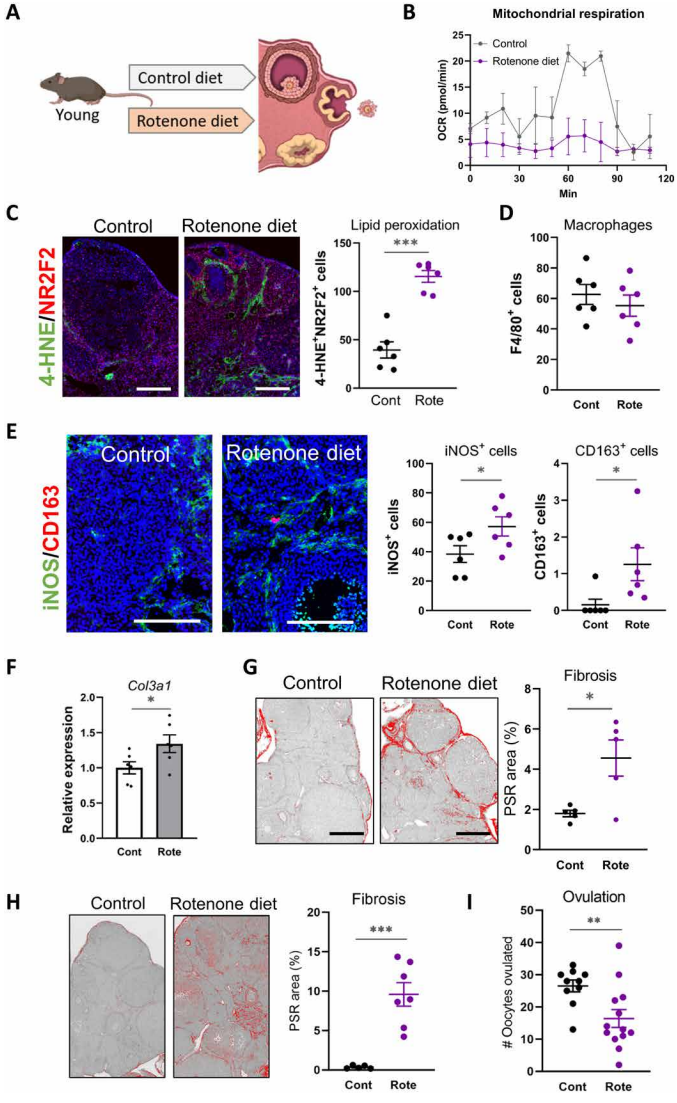

Fig. 9. Rotenone diet induces fibrosis in the ovarian stroma. (**A**) Schematic of experimental design with young lean mice administered with rotenone (150 ppm in diet; to disrupt oxidative phosphorylation) or matched control diet for 3 weeks (B to G) or 5 weeks (H and I), followed by gonadotropin treatment to induce ovulation. (**B**) Kinetics of OCR in ovarian stromal cells using the Seahorse XF Analyzer. Values represent means ± SEM of $n = 2$ replicate wells containing cells pooled from four mice. Scale bar, 200 μm. (**C**) Representative immunodetection of 4-HNE (oxidation marker; green) colocalized with stromal marker NR2F2 (red) in ovaries of mice fed rotenone (Rote) or matching control (Cont) diet, and quantification of double-positive cells (right). (**D**) Macrophages were localized by immunohistochemistry using anti-F4/80 antibody, and positive cells were counted. (**E**) Macrophage phenotyping in ovarian sections using anti-iNOS (M1 marker; green) and anti-CD163 (M2 marker; red), followed by quantification of each cell type (right). Scale bars, 200 μm. (**F**) Gene expression of *Col3a1* in ovarian stroma. $n = 6$ samples of stromal cells from individual mice. (**G**) Representative PSR-stained ovarian sections from mice fed rotenone diet or control and quantification of fibrosis area (right). Values represent means ± SEM of ovaries from $n = 5$ mice per group. Scale bars, 200 μm. (**H**) Representative PSR-stained ovarian sections from mice fed rotenone diet or control (for 5 weeks) and quantification of fibrosis area (right). Values represent means ± SEM of ovaries from $n = 5$ or $n = 7$ mice per group. (**I**) Number of ovulated oocytes in mice fed rotenone diet or control for 5 weeks. Values represent means ± SEM of $n = 10$ or $n = 13$ mice per group. $^*P < 0.05$, $^{**}P < 0.01$, and $^{***}P < 0.001$ by two-tailed *t* test.

modest but significant increase in the collagen-positive area, indicating that ovarian fibrosis was initiated by rotenone diet (Fig. 9G). Separate cohorts were fed the rotenone diet for 5 weeks, and in these mice, ovarian collagen deposition was even more pronounced (Fig. 9H). Furthermore, although ovulation was not reduced in mice fed rotenone for 3 weeks (39.9 ± 2.6 oocytes versus 30.2 ± 2.8 in controls; $n = 24$ mice per group), exposure for 5 weeks resulted in impaired ovulation (Fig. 9I). These results indicate that mitochondrial dysfunction alone can instigate the fibrosis cascade within the ovarian stroma, by inducing downstream oxidative damage, shifting macrophage phenotype, and up-regulating collagen deposition. These mechanisms are illustrated schematically in Fig. 10.

DISCUSSION

This study demonstrates that mitochondrial dysfunction is an underlying causative trigger of ovarian fibrosis: a profound change in tissue architecture of the ovary that is not well understood but is increasingly linked with constrained follicle growth, anovulation, and infertility. We have shown that targeting ovarian fibrosis with pharmaceuticals (specifically pirfenidone and BGP-15) can extend ovarian ovulatory function, particularly in the context of reproductive aging when oocyte number is extremely limited. To our knowledge, this is the first discovery of nonhormonal compounds that could be helpful to extend ovarian function as folliculogenesis and ovulation become disordered in the decade before menopause. That collagen accumulation was linked to the number of ovarian cycles indicates that the ovary is uniquely vulnerable to fibrotic damage, and that this contributes to its early functional demise. Unexpectedly, obesity resulted in a remarkably similar type and degree of cellular damage, inflammation, and fibrotic collagen deposition in the ovarian stroma. This raises the concerning prospect that young obese females experience damage to the ovary that is comparable to the events of perimenopause.

Modulation of mitochondrial bioenergetics is identified as the mechanism that underpins the functional outcomes on ovarian collagen remodeling. Disrupting mitochondrial bioenergetics alone was sufficient to instigate the fibrosis cascade within the ovarian stroma, leading to the same downstream stress responses, as occur with obesity or aging (see Fig. 10). Conversely, BGP-15 mitigated ovarian fibrosis in association with improved mitochondrial bioenergetics and reduced mitochondrial ROS production in isolated stromal cells, consistent with efficacy counteracting mitochondrial dysfunction in other disease models (*27*, *28*, *43*). In vitro assays demonstrate that BGP-15 binds mitochondrial membranes and decreases ROS production by stabilizing complex I/III proteins (*44*) and prevents mitochondrial fragmentation, possibly via Opa1-mediated fusion (*45*). Pirfenidone has been observed to exhibit similar mitochondrial effects in models of lung fibrosis, specifically pirfenidone treatment–reduced ROS and superoxide production by aged mouse macrophages (*46*) and human lung fibroblasts (*47*). Metformin and MitoQ are well known to influence mitochondrial bioenergetics (*48*, *49*), and both compounds reduced oxidative stress in ovarian stromal cells of obese mice (fig. S6D). Metformin has been observed to normalize mitochondrial function, suppress collagen secretion, and lessen tissue fibrosis in a mouse model of lung fibrosis (*50*), and in ovaries of postmenopausal women, metformin use was associated with fewer M2-like immune cells and reduced collagen deposition (*4*). Thus, the drugs we show to be effective in reversing ovarian fibrosis likely converge on related metabolic pathways that are upstream of oxidative stress and inflammation.

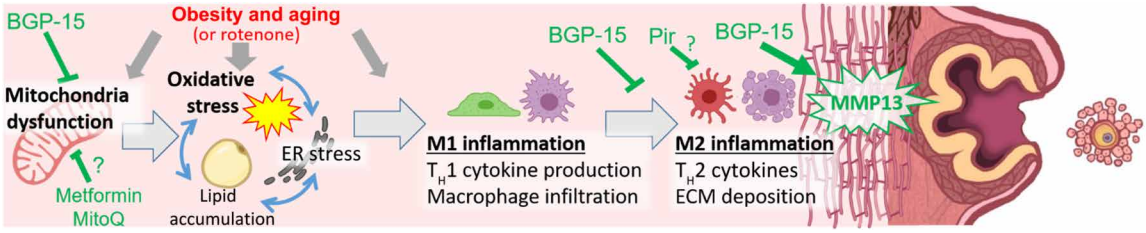

Fig. 10. Summary of findings and proposed mechanisms that cause fibrosis in the ovary and that can be targeted to remove excess collagen and promote ovulation. Mitochondrial dysfunction (as occurs with obesity, aging, or rotenone toxicant) is linked to a cascade of intracellular stress pathways within the ovarian stroma, particularly oxidative stress, which trigger proinflammatory (M1) and anti-inflammatory (M2) responses resulting in fibrotic collagen deposition (vertical red line pattern). BGP-15 treatment of obese or reproductively old female mice improves mitochondrial activity in ovarian stromal cells, reduces oxidative stress, and dampens M2 inflammation. BGP-15 treatment also results in MMP13 protease induction, collagen removal, and improved oocyte release. Mice treated with pirfenidone (Pir), metformin, or MitoQ also exhibit reduced ovarian fibrosis, but whether the mechanisms are identical to those of BGP-15 remains to be determined.

Downstream of mitochondrially driven oxidative stress, we identified distinct shifts in ovarian macrophage phenotype concurrent with collagen deposition. Obesity and aging (and rotenone diet) were associated with increased numbers of inflammatory ($iNOS^+$) M1 macrophages, as well as more anti-inflammatory ($CD163^+$) M2 macrophages that have known roles in stimulating fibrotic collagen deposition by stromal fibroblasts and that characterize wound healing (*13*, *51*). BGP-15 treatment, conversely, constrained the M2 phenotype while not affecting total macrophage numbers. This is most likely due to reduced oxidative damage within the ovarian microenvironment, alleviating the inflammatory signals (i.e., IL-6, Tgfb1, and IL-4; see Fig. 7), which drive M2 macrophage differentiation during fibrosis onset (*41*, *51*). BGP-15 may also act directly on tissue macrophage populations to affect polarization. Compared to M1 macrophages, M2 macrophages are highly dependent on mitochondrial metabolism (*52*) and distinct metabolic reprogramming occurs as macrophages shift to phenotypes that mediate tissue repair (*53*). Hence, by influencing mitochondrial bioenergetics specifically in ovarian macrophages, BGP-15 or other therapeutics including pirfenidone could influence their matrix-remodeling functions. In support of this, MMP13 protease is markedly up-regulated in response to BGP-15, including in macrophages.

Increased stromal collagen deposition was directly correlated with reduced ovulation capacity, presumably due to the increased collagen surrounding the follicles, forming a rigid barrier that hinders the proteolytic remodeling necessary for folliculogenesis and oocyte release. Follicle growth requires extensive remodeling of the surrounding extracellular matrix in order for volume to massively increase (i.e., human follicle size increases 10^6-fold to ~4 cm^3) in the lead up to follicular rupture. Biophysical assessments of ovaries from reproductively old mice (14 to 17 months) demonstrates that they are rigid (*5*), and increasing rigidity around follicles cultured in vitro impairs growth (*54*, *55*). At ovulation, induction of MMPs is required for collagen degradation and follicular rupture (*56*–*58*). Thus, up-regulation of MMP13 by BGP-15 is a probable mechanism by which ovulation is facilitated. Preliminary observations indicate that MMP13 is up-regulated by metformin and MitoQ in the ovaries of obese mice (fig. S6E), but the cellular origins, mechanisms of induction, and whether this protease is the mediator of improved ovarian function require further investigation. MMP13-null mice exhibit increased susceptibility to liver fibrosis and wound-healing defects (*59*, *60*) that, combined with our observations in the ovulating ovary, indicate that induction of MMP13 facilitates extracellular matrix remodeling in specific contexts of exacerbated tissue damage and repair, as occurs with repeated ovarian cycling.

Our demonstration that ovarian fibrosis is acutely modifiable provides translational opportunities and indicates that new attention should be focused on functionality of the stromal compartment. In reproductively older women (i.e., ~35 to 44 years old but premenopausal) or those deemed "nonresponders," the ovaries produce few oocytes even when the presence of healthy follicles is predicted by anti-Mullerian hormone levels and high doses of gonadotropins are given (*61*–*63*). Similarly, obese women have high rates of IVF cycle cancellation due to failed follicle growth responses to hormones (*64*, *65*). Our preclinical studies indicate that improving mitochondrial bioenergetics and reducing collagen deposition within the underlying ovarian stroma will be beneficial toward facilitating follicle growth and maturation in women seeking pregnancy.

Perhaps even more important, however, is accumulating evidence that ovarian fibrosis generates a tissue matrix environment permissive to ovarian cancer, and the exciting concept that minimizing ovarian fibrosis could be a strategy to reduce ovarian cancer risk (*66*). Thus, although metformin did not improve ovulation in reproductively old mice (at least at the dose and timing used here), the capacity to reduce ovarian oxidative damage and collagen deposition is clinically relevant because it provides a mechanistic explanation to substantiate similar observations in ovaries of postmenopausal women (*4*) and indicates that metformin can acutely reverse (and not just prevent) ovarian fibrosis. Last, our direct comparison of nulliparous versus multiparous females demonstrates that ovarian fibrosis is a direct result of repeated cycles of follicular rupture and repair, and not an inevitable consequence of aging. This provides fundamental new insight into the underlying basis for the long known correlation between number of cumulative ovulations and ovarian cancer (*67*), and could influence choice between contraceptives that block follicular rupture (and presumably ovarian fibrosis) versus those that do not. Recent epidemiological studies find that hormonal contraceptive use (which suppresses ovulation) is associated with later natural menopause (*68*, *69*).

Collectively, our findings provide new insight into the mechanism of premature ovarian dysfunction that occurs in premenopausal women and with obesity. We identify the interacting metabolic and inflammatory stress pathways that drive fibrotic collagen deposition resulting in impaired ovulation. These processes could be reversed with existing drugs, creating an opportunity to improve fertility and prolong normal ovarian function in women.

MATERIALS AND METHODS

Animals, hormone treatment, and drug administration

All experiments were approved by the University of Adelaide Animal Ethics Committee and conducted in accordance with the Australian Code of Practice for the Care and Use of Animals for Scientific Purposes (ethics approval numbers: M-2017-116, M-2018-121, and M-2019-086). C57 mice were purchased from the Animal Resources Centre (Canning Vale, Western Australia). Reproductively aged females were 9-month-old retired breeders maintained until 12 to 16 months old depending on the experimental design and as indicated. Young controls were 3 to 6 weeks old. CBAxC57 F_1 male mice used for IVF assays were purchased from the Laboratory Animal Services (University of Adelaide) at 6 to 8 weeks of age.

In experiments investigating the effects of obesity and aging in parallel, mice that were reproductively old or obese, as well as lean young controls, were generated from the same colony (C57BL/6JSfdAnu-Alms1bbb/Apb strain maintained as heterozygous breeding pairs) and fed an identical standard chow diet, as in (*35*). This design ensured that direct comparisons could be made between obese and reproductively aged animals, and strict weight and age criteria were used. Obese mice were homozygous (bbb/bbb) for the "Blobby" mutation of the *Alms1* gene, which results in hyperphagia and thus excess adipose tissue, hyperinsulinemia, and hypercholesterolemia, though maintained on a standard mouse chow diet (*35*). Blobby (bbb/bbb) females have normal fertility before obesity onset (*35*). Females were deemed obese when they weighed at least 36 g, which occurred at around 5 months of age, and wild-type littermates were used in parallel as lean controls. "Old" females were wild-type or heterozygous (+/+ or bbb/+) at 12 months of age, and young females (4 to 5 months old) were used in parallel as controls. While obese females weighed ~42 g on average, old females had a mean body weight of 31 g and controls averaged 26 g.

Pirfenidone (HY-B0673, Med Chem Express, NJ, USA) was given as either intraperitoneal (ip) injection or oral administration (po) in drinking water (see fig. S1) based on published studies in mouse models of fibrosis (*70*–*73*). Pirfenidone was injected (Pir^{ip}) at 100 mg/kg of body weight daily for 4 days. Pirfenidone in drinking water (Pir^{po}) was given at 250 mg/kg of body weight or 500 mg/kg of body weight as indicated, ad libitum for 2 weeks. Estrous cycle was then assessed by vaginal epithelial cell cytology for 10 days, followed by pregnant mare serum gonadotropin (PMSG) and hCG treatment (see figs. S1 and S2).

Nintedanib (HY-50904, Med Chem Express) was dissolved in 10% dimethyl sulfoxide in sesame oil and administered by intraperitoneal injection at 50 mg/kg of body weight daily for 4 days (see fig. S1), with dosing based on previous studies in mouse models of fibrosis (*74*, *75*). Estrous cycle was then assessed by vaginal epithelial cell cytology for 10 days, followed by PMSG and hCG treatment (see figs. S1 and S2).

sgp130Fc (Olamkicept; provided by M. Febbraio) was administered as two injections (intraperitoneally) at 0.5 mg/kg of body weight in saline, with 48 hours between each injection, based on dosing in previous experiments (*19*). Gonadotropin stimulation (PMSG injection) commenced 48 hours after the second gp130Fc dose. Controls were injected with 0.9% saline at the equivalent volume for body weight.

BGP-15 (CAS 66611-37-8, Hangzhou Molcore Biopharmatech Co. Ltd.) was injected intraperitoneally at 100 mg/kg of body weight in saline for 4 days, starting the day before PMSG injection [as in (*35*)]. This treatment regimen does not affect body weight. Controls were injected with 0.9% saline vehicle. Where indicated, in initial experiments, BGP-15 was provided at 100 mg/kg in drinking water ad libitum for 2 weeks before the 4-day injection protocol. See fig. S4 [and supporting studies (*27*–*30*, *35*, *76*)] for dosing rationale.

Metformin (1,1-dimethylbiguanide hydrochloride; D150959, Sigma-Aldrich) was provided to mice at 2 mg/ml in drinking water ad libitum for 2 weeks, before PMSG and hCG treatment. This is a common dose in mouse models of metabolic disease. MitoQ {mitoquinone mesylate: [10-(4,5-dimethoxy-2-methyl-3,6-dioxo-1,4-cyclohexadien-1-yl)decyl](triphenyl)phosphonium methanesulfonate} is a ubiquinone moiety linked to a lipophilic triphenylphosphonium cation by a 10-carbon alkyl chain that preferentially accumulates in mitochondria (*37*). MitoQ (donated by MitoQ Ltd., New Zealand) was delivered at 150 μM in drinking water ad libitum for 2 weeks [see fig. S6 and (*77*) for dosing rationale], before PMSG and hCG treatment.

Mouse chow containing rotenone (150 ppm) was formulated in AIN-93G meal diet by Teklad/Envigo (Madison, WI) exactly as in (*42*). Female mice [CBAxC57 F_1 purchased from Laboratory Animal Services (University of Adelaide)] were provided with rotenone diet or the matched control diet ad libitum for 3 weeks (from 7 to 10 weeks of age) or 5 weeks (from 7 to 12 weeks of age) before PMSG and hCG treatment. This dose is demonstrated to decrease complex I– and complex II–driven respiration without altering oxidative phosphorylation subunit abundance or causing overt physiological effects (*42*).

To stimulate follicle growth and ovulation, all mice used in these studies were injected intraperitoneally with PMSG (#493-10, Lee BioSolutions) at 5 IU/0.1 ml of saline (0.9%) per 12 g of body weight, followed 47.5 hours later by intraperitoneal injection of hCG (Pregnyl, Merck Sharp & Dohme) at 5 IU/0.1 ml of saline per 12 g of body weight. Ovulation occurs at approximately 12 to 13 hours after hCG, and in all experiments, mice were humanely killed by cervical dislocation at exactly 15 hours after hCG.

Tissue collection, ovulation assessment, and IVF

Ovaries and oviducts were collected from each mouse at 15 hours after hCG administration and placed in prewarmed (37°C) α-minimum essential medium (αMEM)–Hepes handling medium. Blood was collected from the heart just after culling and centrifuged to remove blood cells. Serum was stored at −80°C until used for tumor necrosis factor–α (TNFα) and IL-6 cytokine assays (fig. S10). Cumulus oocyte complexes (COCs) were isolated from oviducts and counted to assess ovulation.

For IVF, COCs were isolated by puncturing oviducts using a 30-gauge needle. Whole COC clusters were gently washed twice in prewarmed (37°C) fertilization medium (Vitro Fertilization; Cook Australia, Brisbane, Australia), before being placed in a 100-μl fertilization drop containing the equivalent of 10 μl of capacitated sperm from a male of proven fertility (referred to as "fertilization time"), before being returned to the incubator (37°C, 5% O_2, 6% CO_2) for 4 hours. Following this, fertilized oocytes were cleaned of all excess sperm and cumulus cells via gentle aspiration. At this time, zygotes underwent counting and morphological assessments. Zygote morphology was classified into three groups: "Live" zygotes displayed typical morphology, such as the oocyte occupying most of the space within the zona, no fragmentation, and uniform cytoplasm, while "degenerated" zygotes appeared dark and shrunken within the zona pellucida. When extensive fragmentation was observed, zygotes were classed as "fragmented." Following morphological assessment and counting, zygotes were transferred to a culture dish containing

cleave medium (Vitro Cleave; Cook Australia, Brisbane, Australia; 10 embryos per 20 μl of cleave medium drop) and returned to the incubator until 24 hours after fertilization time. At this time, the number of embryos that successfully reached the two-cell state was scored. The remaining embryos were returned to the incubator until 96 hours after fertilization time when the remaining embryos that had successfully reached the blastocyst stage were scored.

PSR staining, fibrosis area quantitation, and follicle counting

Ovaries were fixed in 4% paraformaldehyde overnight, dehydrated in 70% (v/v) ethanol, embedded in paraffin, and sectioned at 6-μm thickness. Sections were deparaffinized using xylene, hydrated through graded ethanol, and washed with phosphate-buffered saline (PBS). The PSR Stain Kit (24901, Polysciences Inc., Warrington, PA) was used according to the manufacturer's instructions, and ovaries from the same experiment were always stained in the same run. Briefly, deparaffinized and hydrated sections were washed with disulfide water. Sections were then incubated in solution A (phosphomolybdic acid) for 2 min at room temperature (RT), incubated in solution B (PSR F3BA stain) for 1 hour, and washed with disulfide water. Using solution C (0.1 N hydrochloride acid), slides were washed and then dehydrated. Images were captured using Axio Zeiss at light field with a 20× objective.

For every mouse, fibrosis was measured in a single cross section of the entire ovary. The fibrotic area of imaged PSR-stained or collagen-immunolabeled ovaries was quantified using ImageJ software (National Institutes of Health, Bethesda, MD). First, the captured image was converted to a 16-bit image, and a threshold was set on the basis of the staining in the ovaries of the old mice, as in (*6*). This threshold was kept for all images analyzed for each mouse from all groups. Staining intensity was measured only in the stromal cell region by excluding follicles and corpora lutea. Fibrosis area was calculated as staining intensity normalized to stromal tissue area.

For follicle counting, paraffin-embedded ovaries were sectioned at 5-μm thickness. Every fifth slide (totaling 12 to 18 sections per ovary) was stained with hematoxylin and eosin (H&E) and imaged using the NanoZoomer Digital Slide Scanner. Preovulatory follicles were defined as large antral follicles with a COC visible in at least one section. Both ovaries from 8 to 10 mice per group were assessed.

Stromal cell isolation

Ovaries and oviducts were collected from each mouse at 15 hours after hCG administration. To purify stromal cells, corpora lutea were removed by microdissection using a 27-gauge needle, and the remaining ovarian tissue was transferred to αMEM containing 0.1% collagenase (C9722, Sigma-Aldrich). Samples were incubated at 37°C for 30 min with gentle pipette mixing every 5 min. Following this, stromal cells were purified using a 40-μm filter (pluriSelect, Leipzig, Germany), and the medium containing stromal cells was pelleted by centrifugation at 2000 rpm for 5 min and the supernatant was removed. The purity of this cell fraction is demonstrated by negligible expression of granulosa cell– and oocyte-specific mRNAs (Fig. 3B).

Extracellular flux assay using stromal cells

Cellular oxygen consumption rate (OCR) was monitored in real time using the Seahorse Bioscience Extracellular Flux Analyzer (XF96e, Agilent, Santa Clara, CA). Ovarian stromal cells were collected and purified via filtration as above. After washing in Dulbecco's modified Eagle's medium (DMEM) (D5030, Sigma-Aldrich), cell numbers were quantified using Countess II (Invitrogen/Life Technologies, Carlsbad, CA) and diluted to (ideally) 200,000 cells/180 μl of Seahorse assay medium. eXF96 96-well assay plates were coated with fibronectin (5 μg/ml) overnight the day before the assay and washed with DMEM. Each well was then seeded with 180 μl of Seahorse assay medium containing 200,000 cells and incubated at 37°C for 1 hour in the absence of CO_2, before OCR measurements. Assays were performed in 9-min cycles of mix (3 min), wait (3 min), and measure (3 min) as per the manufacturer's recommendations.

For mitochondrial stress test assays, cells were sequentially treated as indicated with oligomycin (1 μM), carbonyl cyanide 4-(trifluoromethoxy) phenylhydrazone (FCCP; 1 μM), and a combination of antimycin A (0.5 μM) and rotenone (0.5 μM). For glycolysis assays, cells were sequentially treated with glucose (10 mM), oligomycin (1 μM), and 2-deoxyglucose (50 mM). To measure fatty acid oxidation, the Seahorse XF Palmitate Oxidation Stress Test Kit (103693-100, Agilent) was used according to the manufacturer's protocol. Replicate wells of stromal cells were treated with either fatty acid–free bovine serum albumin (BSA) (for basal measurements) or palmitate-BSA and then sequentially with oligomycin (1 μM), FCCP (5 μM), and a combination of antimycin A (0.5 μM) and rotenone (0.5 μM). All chemicals were purchased from Sigma-Aldrich except for the Seahorse XF Palmitate Oxidation Stress Test Kit.

Cellular metabolism readouts, such as basal respiration, glycolysis, and ATP production, were determined using the Agilent Seahorse Wave software. Where indicated, mitochondrial stress test data and glycolysis test data were normalized to the first reading of the control group. In fatty acid oxidation tests, data were normalized to replicate wells of cells that were in fatty acid–free BSA and not treated with assay compounds.

Analysis of mitochondrial membrane potential and oxidative stress and PARP1 activity

Stromal cell mitochondrial membrane potential and oxidative stress were measured using JC-1 potentiometric dye (T3168, Invitrogen) and MitoSOX Red (M36008, Invitrogen), respectively, according to the manufacturer's protocols. Briefly, stromal cells were isolated as above in 180 μl of αMEM containing 0.1% collagenase. Following 30 min of incubation at 37°C, 20 μl of 10× TrypLE (A12177, Gibco Life Technologies, Waltham, MA) was added and incubated for 2 min at RT. A further 800 μl of αMEM was added to stop trypsin activity, and 1 μl of deoxyribonuclease (1 mg/ml) (D4263, Sigma-Aldrich) was added. Cells were gently pelleted and then resuspended in 100 μl of αMEM, with a final concentration of 5 μM JC-1 dye or 10 μM MitoSOX Red reagent at 37°C for 30 min while protected from light. Fluorescence in a total of 50,000 cell events per sample was detected by flow cytometry using a FACSCanto II flow cytometer (BD Biosciences, San Jose, CA). Representative examples of the gating strategy are shown in fig. S7.

PARP1 activity was measured using the PARP1 Enzyme Activity Assay (17-10149, Sigma-Aldrich) according to the manufacturer's instructions. Isolated stromal cells were homogenized using PBS(–), and the supernatant was used for the assay, wherein PARP1 converts nicotinamide adenine dinucleotide (NAD^+) to nicotinamide (NAM) that is measured by fluorescence and normalized to total protein.

Immunofluorescence of ovarian tissue sections

Ovaries were frozen in the Tissue-Tek OCT Compound (Sakura Finetek, Torrance, CA) on dry ice. Frozen cryo-sections (10 μm) were mounted

on slides and fixed with 4% paraformaldehyde at RT for 30 min. Sections were blocked with 5% (w/v) BSA in PBS for 1 hour at RT, followed by incubation with the primary antibody (table S1) diluted in 2.5% BSA with 0.15% Triton X-100 in PBS overnight at 4°C. After washing in 0.3% (v/v) Triton X-100 in PBS, slides were incubated with secondary antibody (table S1) diluted in 5% (w/v) BSA-PBS for 2 hours at RT, protected from light. (For double-staining, washed sections were incubated with 5% BSA-PBS again and incubated overnight at 4°C with another primary antibody. Following this, slides were washed with 0.3% Triton X-100–PBS and incubated with secondary antibodies.) After washing, slides were stained with 4′,6-diamidino-2-phenylindole (DAPI) for visualizing nuclei and mounted with a coverslip. Images were acquired using an Axio Zeiss microscope (Carl Zeiss, Oberkochen, Germany) with a 20× objective.

RNA extraction, reverse transcription, and quantitative polymerase chain reaction

Total RNA was obtained from ovarian stromal cells using the RNeasy Mini Kit (QIAGEN Sciences, Germantown, MD) according to the manufacturer's instructions. cDNA was synthesized from 500 ng of extracted RNA using a SuperScript III reverse transcriptase kit (Thermo Fisher Scientific, Waltham, MA). cDNA was used for quantitative polymerase chain reaction (qPCR) with TaqMan methodology, and the primers are listed in table S2. Expression was first normalized to housekeeper *Rpl19*, and fold change was calculated relative to the mean of the control samples.

Measurement of TNFα and IL-6

TNFα and IL-6 were measured in serum and stromal cells using mouse enzyme-linked immunosorbent assay kits (TNFα: ADI-900-047, Enzo Life Sciences, Farmingdale, NY; IL-6: ab100713, Abcam, Cambridge, UK) according to the manufacturer's instructions. Cytokine measurements were normalized to the total protein concentration using the Protein Assay Dye Reagent Concentrate (#5000006, Bio-Rad Laboratories, Hercules, CA).

Western blots

Isolated stromal cells were lysed in lithium dodecyl sulfate (LDS) buffer (Thermo Fisher Scientific) containing 1 μl of β-mercaptoethanol and heated to 65°C for 10 min. Equal volumes of samples were loaded, and proteins were separated by gel electrophoresis at 165 V for 45 min. Protein was transferred onto the polyvinylidene difluoride membrane and blocked with 5% (v/v) BSA in PBS for 2 hours at RT. Primary antibodies (anti-MMP13, 1:500, and anti–histone 3 antibody, 1:1000; table S1) were diluted in 2.5% (w/v) BSA and 0.1% (v/v) Triton X-100 in PBS and incubated overnight at 4°C. After washing in 0.1% Tween 20 (v/v) in PBS for 2 hours, the membrane was incubated with the corresponding secondary antibodies diluted with 2.5% (w/v) BSA-PBS for 1 hour at RT. Membranes were imaged using the Odyssey Imager for fluorescent antibody detection.

Statistics and reproducibility

Statistical analyses of data were performed using R software (www.r-project.org) and GraphPad Prism 9. Each experiment involved multiple cohorts of animals, and data points are from ovaries of individual mice or cells pooled from multiple mice as indicated in the text. All measurements were taken from distinct samples. All bar graphs are shown as means + SEM. Comparisons between control, obese, and old mice were analyzed by one-way analysis of variance (ANOVA). Comparisons between drug-treated mice and vehicle-treated controls were analyzed by unpaired Student's two-tailed *t* test. Correlation between fibrosis and ovulation was by Pearson's test. $P < 0.05$ was considered statistically significant.

SUPPLEMENTARY MATERIALS

Supplementary material for this article is available at https://science.org/doi/10.1126/sciadv.abn4564

View/request a protocol for this paper from *Bio-protocol*.

REFERENCES AND NOTES

1. L. J. Heffner, Advanced maternal age—How old is too old? *N. Engl. J. Med.* **351**, 1927–1929 (2004).
2. F. J. Broekmans, M. R. Soules, B. C. Fauser, Ovarian aging: Mechanisms and clinical consequences. *Endocr. Rev.* **30**, 465–493 (2009).
3. M. J. Faddy, R. G. Gosden, A. Gougeon, S. J. Richardson, J. F. Nelson, Accelerated disappearance of ovarian follicles in mid-life: Implications for forecasting menopause. *Hum. Reprod.* **7**, 1342–1346 (1992).
4. C. W. McCloskey, D. P. Cook, B. S. Kelly, F. Azzi, C. H. Allen, A. Forsyth, J. Upham, K. J. Rayner, D. A. Gray, R. W. Boyd, S. Murugkar, B. Lo, D. Trudel, M. K. Senterman, B. C. Vanderhyden, Metformin abrogates age-associated ovarian fibrosis. *Clin. Cancer Res.* **26**, 632–642 (2020).
5. F. Amargant, S. L. Manuel, Q. Tu, W. S. Parkes, F. Rivas, L. T. Zhou, J. E. Rowley, C. E. Villanueva, J. E. Hornick, G. S. Shekhawat, J. J. Wei, M. E. Pavone, A. R. Hall, M. T. Pritchard, F. E. Duncan, Ovarian stiffness increases with age in the mammalian ovary and depends on collagen and hyaluronan matrices. *Aging Cell* **19**, e13259 (2020).
6. S. M. Briley, S. Jasti, J. M. McCracken, J. E. Hornick, B. Fegley, M. T. Pritchard, F. E. Duncan, Reproductive age-associated fibrosis in the stroma of the mammalian ovary. *Reproduction* **152**, 245–260 (2016).
7. J. N. Mara, L. T. Zhou, M. Larmore, B. Johnson, R. Ayiku, F. Amargant, M. T. Pritchard, F. E. Duncan, Ovulation and ovarian wound healing are impaired with advanced reproductive age. *Aging* **12**, 9686–9713 (2020).
8. T. Umehara, T. Kawai, I. Kawashima, K. Tanaka, S. Okuda, H. Kitasaka, J. S. Richards, M. Shimada, The acceleration of reproductive aging in Nrg1(flox/flox);Cyp19-Cre female mice. *Aging Cell* **16**, 1288–1299 (2017).
9. S. Wang, Y. Zheng, J. Li, Y. Yu, W. Zhang, M. Song, Z. Liu, Z. Min, H. Hu, Y. Jing, X. He, L. Sun, L. Ma, C. R. Esteban, P. Chan, J. Qiao, Q. Zhou, J. C. Izpisua Belmonte, J. Qu, F. Tang, G. H. Liu, Single-cell transcriptomic atlas of primate ovarian aging. *Cell* **180**, 585–600.e19 (2020).
10. N. C. Henderson, F. Rieder, T. A. Wynn, Fibrosis: From mechanisms to medicines. *Nature* **587**, 555–566 (2020).
11. G. Marcelin, A. L. M. Silveira, L. B. Martins, A. V. Ferreira, K. Clément, Deciphering the cellular interplays underlying obesity-induced adipose tissue fibrosis. *J. Clin. Investig.* **129**, 4032–4040 (2019).
12. P. Heukels, C. C. Moor, J. H. von der Thüsen, M. S. Wijsenbeek, M. Kool, Inflammation and immunity in IPF pathogenesis and treatment. *Respir. Med.* **147**, 79–91 (2019).
13. G. F. Vasse, M. Nizamoglu, I. H. Heijink, M. Schlepütz, P. van Rijn, M. J. Thomas, J. K. Burgess, B. N. Melgert, Macrophage-stroma interactions in fibrosis: Biochemical, biophysical, and cellular perspectives. *J. Pathol.* **254**, 344–357 (2021).
14. S. Saito, A. Alkhatib, J. K. Kolls, Y. Kondoh, J. A. Lasky, Pharmacotherapy and adjunctive treatment for idiopathic pulmonary fibrosis (IPF). *J. Thorac. Dis.* **11**, S1740–S1754 (2019).
15. P. Spagnolo, A. Tzouvelekis, F. Bonella, The management of patients with idiopathic pulmonary fibrosis. *Front. Med.* **5**, 148 (2018).
16. C. J. Brewer, A. H. Balen, The adverse effects of obesity on conception and implantation. *Reproduction* **140**, 347–364 (2010).
17. D. E. Broughton, K. H. Moley, Obesity and female infertility: Potential mediators of obesity's impact. *Fertil. Steril.* **107**, 840–847 (2017).
18. F. Lunardi, F. Pezzuto, S. E. Vuljan, F. Calabrese, Idiopathic pulmonary fibrosis and antifibrotic treatments: Focus on experimental studies. *Arch. Pathol. Lab. Med.* **142**, 1090–1097 (2018).
19. M. J. Kraakman, H. L. Kammoun, T. L. Allen, V. Deswaerte, D. C. Henstridge, E. Estevez, V. B. Matthews, B. Neill, D. A. White, A. J. Murphy, L. Peijs, C. Yang, S. Risis, C. R. Bruce, X. J. Du, A. Bobik, R. S. Lee-Young, B. A. Kingwell, A. Vasanthakumar, W. Shi, A. Kallies, G. I. Lancaster, S. Rose-John, M. A. Febbraio, Blocking IL-6 trans-signaling prevents high-fat diet-induced adipose tissue macrophage recruitment but does not improve insulin resistance. *Cell Metab.* **21**, 403–416 (2015).
20. O. J. McElvaney, G. F. Curley, S. Rose-John, N. G. McElvaney, Interleukin-6: Obstacles to targeting a complex cytokine in critical illness. *Lancet Respir. Med.* **9**, 643–654 (2021).
21. A. L. Mora, M. Bueno, M. Rojas, Mitochondria in the spotlight of aging and idiopathic pulmonary fibrosis. *J. Clin. Investig.* **127**, 405–414 (2017).

22. M. M. Quadri, S. S. Fatima, R. C. Che, A. H. Zhang, Mitochondria and renal fibrosis. *Adv. Exp. Med. Biol.* **1165**, 501–524 (2019).
23. N. E. Sunny, F. Bril, K. Cusi, Mitochondrial adaptation in nonalcoholic fatty liver disease: Novel mechanisms and treatment strategies. *Trends Endocrinol. Metab. TEM* **28**, 250–260 (2017).
24. T. Crul, N. Toth, S. Piotto, P. Literati-Nagy, K. Tory, P. Haldimann, B. Kalmar, L. Greensmith, Z. Torok, G. Balogh, I. Gombos, F. Campana, S. Concilio, F. Gallyas, G. Nagy, Z. Berente, B. Gungor, M. Peter, A. Glatz, A. Hunya, Z. Literati-Nagy, L. Vigh Jr., F. Hoogstra-Berends, A. Heeres, I. Kuipers, L. Loen, J. P. Seerden, D. Zhang, R. A. Meijering, R. H. Henning, B. J. Brundel, H. H. Kampinga, L. Koranyi, Z. Szilvassy, J. Mandl, B. Sumegi, M. A. Febbraio, I. Horvath, P. L. Hooper, L. Vigh, Hydroximic acid derivatives: Pleiotropic HSP co-inducers restoring homeostasis and robustness. *Curr. Pharm. Des.* **19**, 309–346 (2013).
25. B. Literati-Nagy, E. Kulcsar, Z. Literati-Nagy, B. Buday, E. Peterfai, T. Horvath, K. Tory, A. Kolonics, A. Fleming, J. Mandl, L. Koranyi, Improvement of insulin sensitivity by a novel drug, BGP-15, in insulin-resistant patients: A proof of concept randomized double-blind clinical trial. *Horm. Metab. Res.* **41**, 374–380 (2009).
26. Z. Literáti-Nagy, K. Tory, B. Literáti-Nagy, A. Kolonics, Z. Török, I. Gombos, G. Balogh, L. Vígh Jr., I. Horváth, J. Mandl, B. Sümegi, P. L. Hooper, L. Vígh, The HSP co-inducer BGP-15 can prevent the metabolic side effects of the atypical antipsychotics. *Cell Stress Chaperones* **17**, 517–521 (2012).
27. D. C. Henstridge, C. R. Bruce, B. G. Drew, K. Tory, A. Kolonics, E. Estevez, J. Chung, N. Watson, T. Gardner, R. S. Lee-Young, T. Connor, M. J. Watt, K. Carpenter, M. Hargreaves, S. L. McGee, A. L. Hevener, M. A. Febbraio, Activating HSP72 in rodent skeletal muscle increases mitochondrial number and oxidative capacity and decreases insulin resistance. *Diabetes* **63**, 1881–1894 (2014).
28. S. B. Ohlen, M. L. Russell, M. J. Brownstein, F. Lefcort, BGP-15 prevents the death of neurons in a mouse model of familial dysautonomia. *Proc. Natl. Acad. Sci. U.S.A.* **114**, 5035–5040 (2017).
29. S. M. Gehrig, C. van der Poel, T. A. Sayer, J. D. Schertzer, D. C. Henstridge, J. E. Church, S. Lamon, A. P. Russell, K. E. Davies, M. A. Febbraio, G. S. Lynch, Hsp72 preserves muscle function and slows progression of severe muscular dystrophy. *Nature* **484**, 394–398 (2012).
30. G. Sapra, Y. K. Tham, N. Cemerlang, A. Matsumoto, H. Kiriazis, B. C. Bernardo, D. C. Henstridge, J. Y. Ooi, L. Pretorius, E. J. Boey, L. Lim, J. Sadoshima, P. J. Meikle, N. A. Mellet, E. A. Woodcock, S. Marasco, T. Ueyama, X. J. Du, M. A. Febbraio, J. R. McMullen, The small-molecule BGP-15 protects against heart failure and atrial fibrillation in mice. *Nat. Commun.* **5**, 5705 (2014).
31. A. P. Snider, J. R. Wood, Obesity induces ovarian inflammation and reduces oocyte quality. *Reproduction* **158**, R79–R90 (2019).
32. R. L. Robker, L. L. Wu, X. Yang, Inflammatory pathways linking obesity and ovarian dysfunction. *J. Reprod. Immunol.* **88**, 142–148 (2011).
33. C. Tatone, F. Amicarelli, M. C. Carbone, P. Monteleone, D. Caserta, R. Marci, P. G. Artini, P. Piomboni, R. Focarelli, Cellular and molecular aspects of ovarian follicle ageing. *Hum. Reprod. Update* **14**, 131–142 (2008).
34. Z. Zhang, F. Schlamp, L. Huang, H. Clark, L. Brayboy, Inflammaging is associated with shifted macrophage ontogeny and polarization in the aging mouse ovary. *Reproduction* **159**, 325–337 (2020).
35. L. L. Wu, D. L. Russell, S. L. Wong, M. Chen, T. S. Tsai, J. C. S. John, R. J. Norman, M. A. Febbraio, J. Carroll, R. L. Robker, Mitochondrial dysfunction in oocytes of obese mothers: Transmission to offspring and reversal by pharmacological endoplasmic reticulum stress inhibitors. *Development* **142**, 681–691 (2015).
36. G. Vial, D. Detaille, B. Guigas, Role of mitochondria in the mechanism(s) of action of metformin. *Front. Endocrinol.* **10**, 294 (2019).
37. M. P. Murphy, R. A. Smith, Targeting antioxidants to mitochondria by conjugation to lipophilic cations. *Annu. Rev. Pharmacol. Toxicol.* **47**, 629–656 (2007).
38. M. J. Rossman, J. R. Santos-Parker, C. A. C. Steward, N. Z. Bispham, L. M. Cuevas, H. L. Rosenberg, K. A. Woodward, M. Chonchol, R. A. Gioscia-Ryan, M. P. Murphy, D. R. Seals, Chronic supplementation with a mitochondrial antioxidant (MitoQ) improves vascular function in healthy older adults. *Hypertension* **71**, 1056–1063 (2018).
39. X. M. Meng, D. J. Nikolic-Paterson, H. Y. Lan, Inflammatory processes in renal fibrosis. *Nat. Rev. Nephrol.* **10**, 493–503 (2014).
40. K. S. Smigiel, W. C. Parks, Macrophages, wound healing, and fibrosis: Recent insights. *Curr. Rheumatol. Rep.* **20**, 17 (2018).
41. B. Kelly, L. A. O'Neill, Metabolic reprogramming in macrophages and dendritic cells in innate immunity. *Cell Res.* **25**, 771–784 (2015).
42. O. A. Lozoya, F. Xu, D. Grenet, T. Wang, S. A. Grimm, V. Godfrey, S. Waidyanatha, R. P. Woychik, J. H. Santos, Single nucleotide resolution analysis reveals pervasive, long-lasting dna methylation changes by developmental exposure to a mitochondrial toxicant. *Cell Rep.* **32**, 108131 (2020).
43. H. Salah, M. Li, N. Cacciani, S. Gastaldello, H. Ogilvie, H. Akkad, A. V. Namuduri, V. Morbidoni, K. A. Artemenko, G. Balogh, V. Martinez-Redondo, P. Jannig, Y. Hedstrom, B. Dworkin, J. Bergquist, J. Ruas, L. Vigh, L. Salviati, L. Larsson, The chaperone co-inducer BGP-15 alleviates ventilation-induced diaphragm dysfunction. *Sci. Transl. Med.* **8**, 350ra103 (2016).
44. K. Sumegi, K. Fekete, C. Antus, B. Debreceni, E. Hocsak, F. Gallyas Jr., B. Sumegi, A. Szabo, BGP-15 protects against oxidative stress- or lipopolysaccharide-induced mitochondrial destabilization and reduces mitochondrial production of reactive oxygen species. *PLOS ONE* **12**, e0169372 (2017).
45. A. Szabo, K. Sumegi, K. Fekete, E. Hocsak, B. Debreceni, G. Setalo Jr., K. Kovacs, L. Deres, A. Kengyel, D. Kovacs, J. Mandl, M. Nyitrai, M. A. Febbraio, F. Gallyas Jr., B. Sumegi, Activation of mitochondrial fusion provides a new treatment for mitochondria-related diseases. *Biochem. Pharmacol.* **150**, 86–96 (2018).
46. M. Plataki, S. J. Cho, R. M. Harris, H. R. Huang, H. S. Yun, K. T. Schiffer, H. W. Stout-Delgado, Mitochondrial dysfunction in aged macrophages and lung during primary streptococcus pneumoniae infection is improved with pirfenidone. *Sci. Rep.* **9**, 971 (2019).
47. Y. Kurita, J. Araya, S. Minagawa, H. Hara, A. Ichikawa, N. Saito, T. Kadota, K. Tsubouchi, N. Sato, M. Yoshida, K. Kobayashi, S. Ito, Y. Fujita, H. Utsumi, H. Yanagisawa, M. Hashimoto, H. Wakui, Y. Yoshii, T. Ishikawa, T. Numata, Y. Kaneko, H. Asano, M. Yamashita, M. Odaka, T. Morikawa, K. Nakayama, K. Kuwano, Pirfenidone inhibits myofibroblast differentiation and lung fibrosis development during insufficient mitophagy. *Respir. Res.* **18**, 114 (2017).
48. M. Faure, M. J. Bertoldo, R. Khoueiry, A. Bongrani, F. Brion, C. Giulivi, J. Dupont, P. Froment, Metformin in reproductive biology. *Front. Endocrinol.* **9**, 675 (2018).
49. M. P. Murphy, Understanding and preventing mitochondrial oxidative damage. *Biochem. Soc. Trans.* **44**, 1219–1226 (2016).
50. S. Rangarajan, N. B. Bone, A. A. Zmijewska, S. Jiang, D. W. Park, K. Bernard, M. L. Locy, S. Ravi, J. Deshane, R. B. Mannon, E. Abraham, V. Darley-Usmar, V. J. Thannickal, J. W. Zmijewski, Metformin reverses established lung fibrosis in a bleomycin model. *Nat. Med.* **24**, 1121–1127 (2018).
51. T. A. Wynn, K. M. Vannella, Macrophages in tissue repair, regeneration, and fibrosis. *Immunity* **44**, 450–462 (2016).
52. A. Batista-Gonzalez, R. Vidal, A. Criollo, L. J. Carreño, New insights on the role of lipid metabolism in the metabolic reprogramming of macrophages. *Front. Immunol.* **10**, 2993 (2020).
53. S. Willenborg, D. E. Sanin, A. Jais, X. Ding, T. Ulas, J. Nüchel, M. Popović, T. MacVicar, T. Langer, J. L. Schultze, A. Gerbaulet, A. Roers, E. J. Pearce, J. C. Brüning, A. Trifunovic, S. A. Eming, Mitochondrial metabolism coordinates stage-specific repair processes in macrophages during wound healing. *Cell Metab.* **33**, 2398–2414.e9 (2021).
54. E. R. West, M. Xu, T. K. Woodruff, L. D. Shea, Physical properties of alginate hydrogels and their effects on in vitro follicle development. *Biomaterials* **28**, 4439–4448 (2007).
55. M. Xu, E. West, L. D. Shea, T. K. Woodruff, Identification of a stage-specific permissive in vitro culture environment for follicle growth and oocyte development. *Biol. Reprod.* **75**, 916–923 (2006).
56. R. Reich, A. Tsafriri, G. L. Mechanic, The involvement of collagenolysis in ovulation in the rat. *Endocrinology* **116**, 522–527 (1985).
57. R. L. Robker, D. L. Russell, S. Yoshioka, S. C. Sharma, J. P. Lydon, B. W. O'Malley, L. L. Espey, J. S. Richards, Ovulation: A multi-gene, multi-step process. *Steroids* **65**, 559–570 (2000).
58. T. E. Curry Jr., K. G. Osteen, The matrix metalloproteinase system: Changes, regulation, and impact throughout the ovarian and uterine reproductive cycle. *Endocr. Rev.* **24**, 428–465 (2003).
59. J. George, M. Tsutsumi, M. Tsuchishima, MMP-13 deletion decreases profibrogenic molecules and attenuates N-nitrosodimethylamine-induced liver injury and fibrosis in mice. *J. Cell. Mol. Med.* **21**, 3821–3835 (2017).
60. N. Hattori, S. Mochizuki, K. Kishi, T. Nakajima, H. Takaishi, J. D'Armiento, Y. Okada, MMP-13 plays a role in keratinocyte migration, angiogenesis, and contraction in mouse skin wound healing. *Am. J. Pathol.* **175**, 533–546 (2009).
61. M. Devesa, R. Tur, I. Rodriguez, B. Coroleu, F. Martinez, N. P. Polyzos, Cumulative live birth rates and number of oocytes retrieved in women of advanced age. A single centre analysis including 4500 women ≥38 years old. *Hum. Reprod.* **33**, 2010–2017 (2018).
62. H. W. Li, V. C. Lee, E. Y. Lau, W. S. Yeung, P. C. Ho, E. H. Ng, Ovarian response and cumulative live birth rate of women undergoing in-vitro fertilisation who had discordant anti-Mullerian hormone and antral follicle count measurements: A retrospective study. *PLOS ONE* **9**, e108493 (2014).
63. Y. Zhang, Y. Xu, Q. Xue, J. Shang, X. Yang, X. Shan, Y. Kuai, S. Wang, C. Zeng, Discordance between antral follicle counts and anti-Müllerian hormone levels in women undergoing in vitro fertilization. *Reprod. Biol. Endocrinol.* **17**, 51 (2019).
64. D. L. Zander-Fox, R. Henshaw, H. Hamilton, M. Lane, Does obesity really matter? The impact of BMI on embryo quality and pregnancy outcomes after IVF in women aged ≤38 years. *Aust. N. Z. J. Obstet. Gynaecol.* **52**, 270–276 (2012).
65. A. MacKenna, J. E. Schwarze, J. A. Crosby, F. Zegers-Hochschild, Outcome of assisted reproductive technology in overweight and obese women. *JBRA Assist. Reprod.* **21**, 79–83 (2017).

66. D. A. Landry, H. T. Vaishnav, B. C. Vanderhyden, The significance of ovarian fibrosis. *Oncotarget* **11**, 4366–4370 (2020).
67. C. La Vecchia, Ovarian cancer: Epidemiology and risk factors. *Eur. J. Cancer Prev.* **26**, 55–62 (2017).
68. A. A. R. Lay, C. F. do Nascimento, B. L. Horta, A. D. P. C. Filho, Reproductive factors and age at natural menopause: A systematic review and meta-analysis. *Maturitas* **131**, 57–64 (2020).
69. D. Appiah, C. C. Nwabuo, I. A. Ebong, M. F. Wellons, S. J. Winters, Trends in age at natural menopause and reproductive life span among US women, 1959-2018. *JAMA* **325**, 1328–1330 (2021).
70. R. Meier, C. Lutz, J. Cosín-Roger, S. Fagagnini, G. Bollmann, A. Hünerwadel, C. Mamie, S. Lang, A. Tchouboukov, F. E. Weber, A. Weber, G. Rogler, M. Hausmann, Decreased fibrogenesis after treatment with pirfenidone in a newly developed mouse model of intestinal fibrosis. *Inflamm. Bowel Dis.* **22**, 569–582 (2016).
71. C. Polydorou, F. Mpekris, P. Papageorgis, C. Voutouri, T. Stylianopoulos, Pirfenidone normalizes the tumor microenvironment to improve chemotherapy. *Oncotarget* **8**, 24506–24517 (2017).
72. M. Reddy, L. Fonseca, S. Gowda, B. Chougule, A. Hari, S. Totey, Human adipose-derived mesenchymal stem cells attenuate early stage of bleomycin induced pulmonary fibrosis: Comparison with pirfenidone. *Int. J. Stem Cells* **9**, 192–206 (2016).
73. C. Van Erp, N. G. Irwin, A. J. Hoey, Long-term administration of pirfenidone improves cardiac function in mdx mice. *Muscle Nerve* **34**, 327–334 (2006).
74. V. Laszlo, Z. Valko, I. Kovacs, J. Ozsvar, M. A. Hoda, T. Klikovits, D. Lakatos, A. Czirok, T. Garay, A. Stiglbauer, T. H. Helbich, M. Gröger, J. Tovari, W. Klepetko, C. Pirker, M. Grusch, W. Berger, F. Hilberg, B. Hegedus, B. Dome, Nintedanib is active in malignant pleural mesothelioma cell models and inhibits angiogenesis and tumor growth in vivo. *Clin. Cancer Res.* **24**, 3729–3740 (2018).
75. B. Öztürk Akcora, G. Storm, J. Prakash, R. Bansal, Tyrosine kinase inhibitor BIBF1120 ameliorates inflammation, angiogenesis and fibrosis in CCl4-induced liver fibrogenesis mouse model. *Sci. Rep.* **7**, 44545 (2017).
76. J. Chung, A. K. Nguyen, D. C. Henstridge, A. G. Holmes, M. H. Chan, J. L. Mesa, G. I. Lancaster, R. J. Southgate, C. R. Bruce, S. J. Duffy, I. Horvath, R. Mestril, M. J. Watt, P. L. Hooper, B. A. Kingwell, L. Vigh, A. Hevener, M. A. Febbraio, HSP72 protects against obesity-induced insulin resistance. *Proc. Natl. Acad. Sci. U.S.A.* **105**, 1739–1744 (2008).
77. R. A. Gioscia-Ryan, T. J. LaRocca, A. L. Sindler, M. C. Zigler, M. P. Murphy, D. R. Seals, Mitochondria-targeted antioxidant (MitoQ) ameliorates age-related arterial endothelial dysfunction in mice. *J. Physiol.* **592**, 2549–2561 (2014).

Acknowledgments: We acknowledge the technical assistance and expert advice of H. Connaughton, M. Gonzalez, and D. (Thao) Dinh. W. Tilley contributed constructive comments on the manuscript. BioRender was used to create the schematics. **Funding:** This work was supported by National Health and Medical Research Council 2013362 (to R.L.R.), National Health and Medical Research Council APP1165633 (to R.L.R. and J.C.), Japanese Society for the Promotion of Science JSPS/OT/300111 (to T.U.), National Health and Medical Research Council APP1130364 (to R.L.R., D.L.R., and J.C.), Japanese Society for the Promotion of Science (JSPS) 19H03108 (to M.S.), National Health and Medical Research Council Research Fellowship APP1117975 (to R.L.R.), and National Health and Medical Research Council Investigator Grant APP1194141 (to M.A.F.). **Author contributions:** Conceptualization: T.U., M.S., and R.L.R. Methodology: T.U., Y.E.W., E.A., A.M., E.J.W., and K.M.S. Investigation: T.U., Y.E.W., E.A., A.M., E.J.W., and K.M.S. Resources: M.A.F. Visualization: T.U., Y.E.W., and R.L.R. Supervision: M.S., D.L.R., and R.L.R. Acquisition of funding: T.U., J.C., and R.L.R. Writing—original draft: T.U. and Y.E.W. Writing—review and editing: T.U., Y.E.W., K.M.S., J.C., M.A.F., D.L.R., and R.L.R. **Competing interests:** M.A.F. is the chief scientific officer of NGene. R.L.R. is an inventor on a pending patent related to this work filed by the University of Adelaide (AU2018337761A1; filed on 21 September 2018, published on 7 May 2020). The authors declare no other competing interests. **Data and materials availability:** All data needed to evaluate the conclusions in the paper are present in the paper and/or the Supplementary Materials.

Submitted 2 December 2021
Accepted 3 May 2022
Published 17 June 2022
10.1126/sciadv.abn4564